To the Graduate Council:

I am submitting herewith a dissertation written by Madhuri V. Salvi entitled "Some Thermodynamic Properties of Ethylene Glycol $(CH_2OH)_2/(CH_2OD)_2$ and their Solutions with Nitromethane : Isotope Effects." I have examined the final copy of this dissertation for form and content and recommend that it be accepted in partial fulfillment of the requirements for the degree of Doctor of Philosophy, with a major in Chemistry.

W. Alexander Van Hook, Major Professor

We have read this dissertation
and recommend its acceptance:

Charlie R. Brooks

John E Bloor

Charles L. Feigerle

Accepted for the Council:

Vice Provost
and Dean of The Graduate School

SOME THERMODYNAMIC PROPERTIES OF ETHYLENE GLYCOL $(CH_2OH)_2/(CH_2OD)_2$ AND THEIR SOLUTIONS WITH NITROMETHANE : ISOTOPE EFFECTS

A Dissertation

Presented for the

Doctor of Philosophy

Degree

The University of Tennessee, Knoxville

Madhuri V. Salvi

December 1989

Copyright © Madhuri V. Salvi, 1989
All rights reserved

Dedication

This dissertation is dedicated to my father (late) Shri. Vasant Sitaram Salvi whose loving memory has been a constant source of inspiration.

Acknowledgments

I wish to thank my major professor, Alexander Van Hook for his instruction, support, and encouragement throughout this research. During these years as his student I tried to learn to conduct meticulous experiments in thermodynamics. Outside the realms of physical chemistry he and his wife Nancy have been like parents to me.

My acknowledgement goes to my committee members for their advice and critical reading of the final manuscript. The financial support provided by the Department of Chemistry and funding from NSF and DOE is gratefully acknowledged.

I am grateful to the following people for their friendship as well as very important practical tips and discussions in the lab. They are Dr. Rajiv Singh, Dr. Zorawar Singh Kooner, Bettyann Williams, and Dr. Jerzey Szydlowski.

Finally a very special "thank you" to my husband Ravindra Narkhede for his patience and strength and his infinite help in the typing and preparation of this dissertation, and to my family for giving me this opportunity and for their love and constant support.

Abstract

The isotope effect on some PVT properties of ethylene glycol have been measured from room temperature up to $574K$. The results have been discussed in terms of the well established statistical mechanical theory of condensed phase isotope effects (CPIE).

The co–existence curve of $(CH_2OH)_2$+ nitromethane system and it's isotopic variant, $(CH_2OD)_2$+ nitromethane has been measured near the upper critical solution temperature and from 1 atmosphere to 50 MPa. The effects of pressure and isotopic substitution on the co–existence curve parameters have been discussed using classical mean field and scaling theories of critical phemomena. When applicable, an attempt has been made to rationalize the observed isotope and pressure effects on the critical parameters by applying the theory of condensed phase isotope effects.

TABLE OF CONTENTS

CHAPTER		PAGE
1. Introduction		**1**
1.1	Critical Phenomenon	3
1.2	Isotope Effect	9
1.3	Isotope Effects on PVT Properties	10
1.3.1	Vapor Pressure Isotope Effects (VPIE)	11
1.3.2	Origin of the Molar Volume Isotope Effect (MVIE)	16
2. Experimental		**18**
2.1	CST Measurements	18
2.1.1	Choice of System	18
2.1.2	Materials	19
2.1.3	Experimental Setup	20
2.1.4	Detection of Phase Transition	22
2.1.5	Data Acquisition	23
2.1.6	Experimental Procedure	24
2.2	Vapor Pressure, Molar Volume, and Compressibility Measurements	24
2.2.1	Apparatus	25
2.2.2	Experimental Procedure	28

CHAPTER PAGE

3. Experimental Results **30**

3.1 Vapor Pressure 30

3.1.1 Vapor Pressure Isotope Effects (VPIE) 38

3.2 Molar Volumes, Compressibilities, and Expansivities 41

3.2.1 Molar Volumes 43

3.2.2 Compressibilities 44

3.2.3 Expansivities 50

3.2.4 Isotope Effects 50

3.3 Critical Solution Temperature (CST) 58

4. Discussion **71**

4.1 VPIE and MVIE 71

4.2 Coexistence curve parameters and their isotope effects 89

4.2.1 Critical Exponent β 89

4.2.2 Critical Concentration X_c 94

4.2.3 Critical Temperature T_c 94

4.2.4 Critical Amplitude A 98

4.2.5 Slope of the Critical Line dT_c/dP 99

5. Conclusion **104**

BIBLIOGRAPHY **106**

CHAPTER PAGE

APPENDIX 114

Calibration of Thermometers 115

VITA 117

LIST OF TABLES

TABLE		PAGE
3.1	Vapor pressure data for $(CH_2OH)_2/(CH_2OD)_2$	31
3.2	Equation (1) parameters	35
3.3	Antoine equation parameters	36
3.4	Parameters for the Chebyshev polynomial	36
3.5	VPIE for $(CH_2OH)_2/(CH_2OD)_2$	39
3.6	Parameters for Eqn. 3.9: $\ln V_T(m^3/mol) = \sum_{i=0}^{2} A_i(P - P^0)^i$	45
3.7	Parameters for Equation 3.12	47
3.8	Parameters of Eqn. 3.19	52
3.9	Orthobaric MVIE's for ethylene glycol	56
3.10	Phase separation data for $(CH_2OH)_2 + CH_3NO_2$ system	59
3.11	Least Squares Fit of Phase Separation Data for $(CH_2OH)_2 + CH_3NO_2$ System	65
3.12	Phase separation data for $(CH_2OD)_2 + CH_3NO_2$ System	68
3.13	Least Squares Fit of Phase Separation Data for $(CH_2OD)_2 + CH_3NO_2$ System	70
4.1	Assignment of the vibrational spectrum of ethylene glycol	73
4.2	Various terms in Eqn. 4.13	81
4.3	Fits of phase separation data for $(CH_2OH)_2 + CH_3NO_2$ with classical expression	92

TABLE PAGE

4.4 UCST Parameters For Some Solutions 94

A.1 Calibration of the platinum resistance thermometer (CST) . . . 115

A.2 Calibration of the platinum resistance thermometer (PVT) . . . 116

LIST OF FIGURES

FIGURE		PAGE
1.1	PVT surface for a pure fluid	4
1.2	T–X–P surface at a liquid–liquid phase transition	6
2.1	Critical solution temperature apparatus	21
2.2	P–V–T Apparatus	26
3.1	Plot of $\ln P'$ vs $1/T$	32
3.2	Plot of $\ln P$ vs $1/T$	33
3.3	Deviation plots	37
3.4	VPIE plot	40
3.5	VPIE for $T > 400K$	42
3.6	Plot of orthobaric molar volumes	46
3.7	Plot of compressibilities	49
3.8	MVIE for $(CH_2OH)_2/(CH_2OD)_2$	53
3.9	Coexistence curves at atmospheric pressure	64
4.1	Orthobaric projection of the $T, \ln(V)$ surfaces of $(CH_2OH)_2/(CH_2OD)_2(- : (CH_2OH)_2, -- : (CH_2OD)_2)$	84
4.2	Extension of the orthobaric projection of the T, $\ln(V)$ towards T_c	86

CHAPTER 1

Introduction

The properties of a liquid and its vapor in equilibrium, become more and more similar as the temperature is raised until at the critical temperature the difference disappears. Loss of spontaneous magnetization for ferromagnets at the Curie temperature, superfluid behaviour of ^{4}He at the lambda point, order–disorder transitions in binary alloys, and consolute points in binary liquid mixtures all exhibit similar behaviour. Early theories, the Van der Waal's theory of the liquid–vapor critical point, the Curie–Weiss theory of ferromagnetism, the Bragg–Williams and Bethe theory of order–disorder phenomena, give a good qualitative picture of critical phenomena, but fail to quantitatively explain phase equilibria near critical points. Moreover, as shown by Uhlenbeck [1] all these theories are based on the assumption that the attractive forces between the molecules which produce the cooperative effects are very long range, and in fact are of the same order as that of the fluctuations. This assumption fails at the critical point. The ordered phase below the critical point can be characterised by an order parameter that goes to zero at the critical point. In all cases a "response function" of the order parameter (specifying the response of the system to an external stress) diverges at the critical point, causing large scale fluctuations

of the order parameter. These fluctuations increase exponentially as the critical point is approached, and there exist anamolies in thermodynamic functions which result in divergence to infinity for functions such as specific heat, magnetic susceptibility, compressibility, correlation length, etc. The phenomenon of critical opalescence also falls into this category. These critical fluctuations are difficult to handle theoretically. The only exact mathematical solution of this phenomenon has been the famous solution by Onsager of the 2–dimensional Ising lattice in 1944, giving results which were in basic disagreement with the classical calculations. The latest phase in the theoretical understanding of critical phenomena was initiated in 1971 by Wilson [2,3,4] whose application of the renormalisation group theory to the critical region provided "respectability" to the field of critical phenomena [5].

The consolute point at which two liquids become miscible in all proportions is thermodynamically isomorphic to the critical phenomena mentioned above. Liquid binary mixtures seem to be ideal candidates for comparison with theory. They are not subject to strains and dislocations as solids are, and moreover, they can be studied at convenient temperatures and pressures. Therefore a large amount of the experimental effort in critical phenomena has been directed towards binary liquid systems.

As mentioned above, various thermodynamic properties diverge in the immediate vicinity of the critical point. Properties that diverge to infinity or converge

to zero at the critical point are expressed in terms of an exponential law,

$$f(t) = at^{\beta}(1 + bt^{\delta} + \cdots)$$

where β is called the critical exponent of quantity $f(t)$ and it describes the anamolous asymptotic behaviour of the property $f(t)$ near the critical point, $t = |T - T_c|/T_c$ is the reduced temperature and expresses the distance from the critical point; a is a system dependent amplitude constant.

1.1 Critical Phenomenon

The first theoretical model describing a critical point was that of Van der Waals. His equation of state

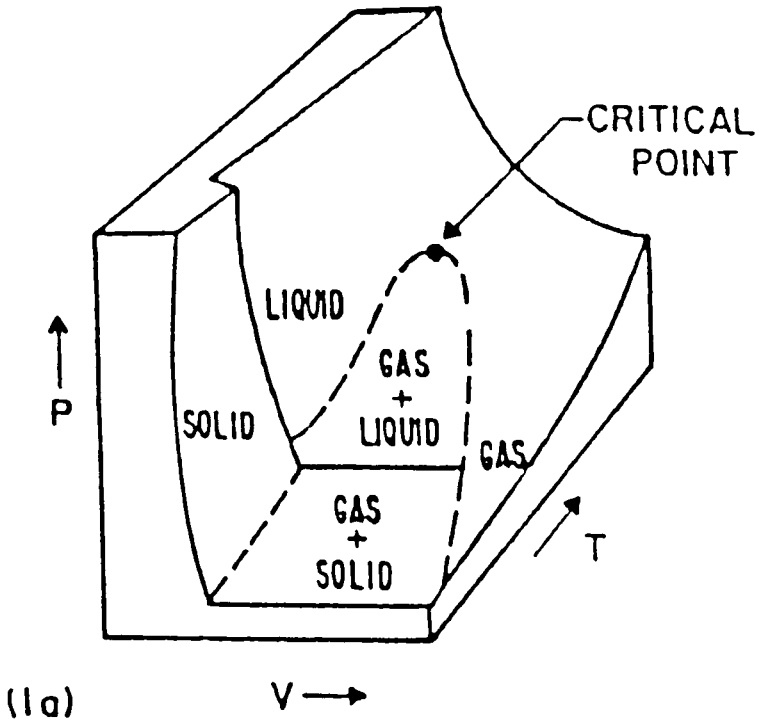
$$(p + a/v^2)(v - b) = RT \tag{1.1}$$

indicates a critical point described by

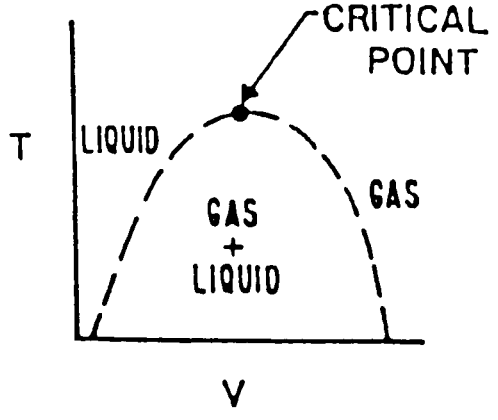
$$(dP/dV)T_c = (d^2P/dV^2) = 0 \qquad (d^3P/dV^3)T_c > 0 \tag{1.2}$$

The isotherms given in Fig. 1.1(a) show that below T_c, two phases with different molar volumes coexist at the same pressure. Figure 1.1(b) shows the projection of the P–V diagram of Fig. 1.1(a) onto the TV plane. It is this projection that we will find useful for our analogy with liquid–liquid critical phenomenon.

Van der Waals description of phase equilibria [1] is one of the so called classical or mean field theories, which can be extended to liquid–liquid equilibria of



(1a)



(1b)

Figure 1.1: (a) Pressure–volume–temperature surface for a pure fluid (b) Temperature–volume projection of a pure fluid PVT surface

binary systems. By Gibb's phase rule, addition of a second component incorporates an additional degree of freedom. Thus the free energy function previously described by $G(T, V)$ becomes $G(T, P, X)$ and the co–existence curve and critical points in TV space become the co–existence surface and critical line in T, X, P space. On applying an additional constraint of fixing a variable, say pressure, we get back a co–existence curve and critical point in TX space. This is indicated in Fig. 1.2(a) which shows two different isobars.

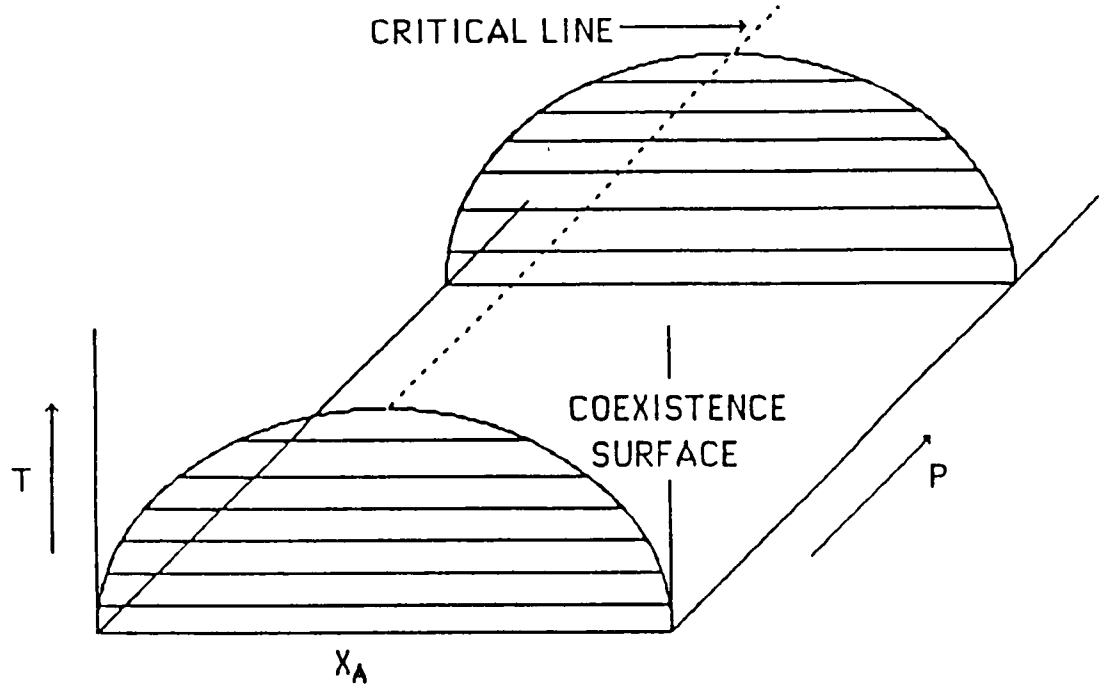
Two formalisms are generally applied to aid in the understanding of the $T - X$ diagrams. Far from the critical point, in the region uncomplicated by long range fluctuations, mean field theory can be applied. In the mean field approach [6] some model or theory is used to generate expressions for the free energy G, as a function of T, P, X etc. $G = G(T, P, X_1, X_2)$. The analyticity of such a function ensures that the derivatives of the free energy functions are real and non–zero at all points. Such a function can be expressed by a Taylor expansion around the critical point T_c. This leads in the limit to the prediction $\beta = 0.5$, for β the critical exponent. Then, applying the classical critical point conditions, *viz*,

$$\left(\frac{d^2G}{dX^2}\right)_{T_c,P} = 0 \tag{1.3}$$

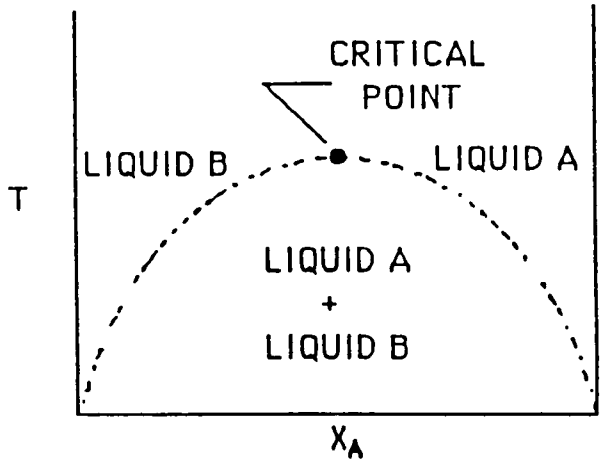
$$\left(\frac{d^3G}{dX^3}\right)_{T_c,P} = 0 \tag{1.4}$$

$$\left(\frac{d^4G}{dX^4}\right)_{T_c,P} > 0 \tag{1.5}$$

the shape of the diagram is deduced. Comparisons with experiment can be used



(2a)



(2b)

Figure 1.2: (a) Temperature–composition–pressure surface at a liquid–liquid phase transition (b) Constant pressure phase diagram for a liquid–liquid phase separation. The temperature and composition at the critical point are termed the critical temperature and critical composition

to test the model.

If we describe the $T - X$ diagram near the critical point by the relation,

$$|X' - X''| = A_1 t^{\beta}(1 + A_2 t^{0.5} + A_3 t + \cdots) \tag{1.6}$$

where $X' - X''$ is the difference in the compositions of the conjugate phases (the order parameter); X being the mole fraction of the component in equilibrium phases $'$ and $''$, modern non–classical theories [2,7] show β to be approximately $1/3$, well below the "classical" $1/2$. Beginning with Greer's [7,8] work in 1975 for the system isobutyric acid + water, experimental values of β for varied binary systems have been reported to be spread between 0.315 to 0.338. These include the systems $C_6H_{12} + CH_3OH$ ($\beta = 0.33$) [9], $C_6H_{12} + CH_3CN$ ($\beta = 0.33$) [10], $CS_2 + CH_3NO_2$ ($\beta = 0.315$) [11], CCL_4 + Perfluoroheptane ($\beta = 0.3197$) [12],as well as many others. The limiting value of β for the region $0 < t < 10^{-3}$ is 0.33. Values other than 0.33 are possible when the phase diagram is considered over a broad temperatue range [13,14,15], that is in other than the limiting case. We will show in a later discussion that the non–classical as well as the classical scaling representations can be applied to describe the co–existence curve over the entire range $0 < t < 0.02$.

The most precise technique for measuring β in binary mixtures is the single sample technique. In this method a single sample is made at the critical concentration, and the equilibrium concentrations in the two co–existing phases are measured by refractive index, dielectric constant, conductivity or density measurements.The value of β thus obtained is very precise, usually within ± 0.001.

The other method to determine β is the multiple sample method wherein several mixtures of known composition are prepared and their phase transition temperatures measured. With this method the critical concentration can be determined independent of the other parameters. However, maintaining the exact low level of impurities in all the samples poses a major problem. The hypersensitivity of T_c to impurity was noticed over 50 years ago by Timmermans [16] and still receives attention [17,18,19]. The two techniques are compared in detail by Stein and Allen [20].

The effect of pressure on liquid–liquid phase equilibria has been studied quite extensively. For almost all cases the pressure dependence of the critical solution temperature (CST) is small and dT_c/dP only rarely exceeds $\pm 0.2^o/bar$. But these older experiments were not designed to obtain the critical parameters. Also, there was relatively low emphasis on temperature control, impurity control, and concentration measurement. Hence these results cannot be used to gain unequivocal information about the critical parameters. The limiting value of the exponent β is now accepted as a universal constant ($\beta = 0.326 \pm 0.011$). The Ginzburg criterion [21] gives the approximate reduced temperature t_g below which the non–classical scaling approach is expected to be correct. For a wide variety of phenomena $t_g = 10^{-3}$ (upper limit). In a recent review Gopal [22] presents several examples that confirm that this limit is also true in the case of the liquid–liquid critical point. Gopal *et al* then point out that the question remains whether the same asymptotic range would hold at higher pressures.

This question has been discussed by several authors [23,24], but many questions remain.Therefore, accurate measurements at higher pressures for binary systems are needed.

1.2 Isotope Effect

Isotope effects on critical solution tempearatures (CST) were first reported in 1934 [25]. Rabinovitch [26] was the first to try to rationalise the observed isotope effect (IE). He noticed that the change in CST on deuteration of polar groups is usually positive $(T_D - T_H) > 0$ and is in a direction opposite to that on deuteration of non–polar groups. This has recently been confirmed by Fenby [27] and Woermann [28]. To date there has been little attempt to give a quantitative theory for the observed isotope effects. Very accurate data is required to interpret this effect. The literature shows a handful of experiments designed to obtain isotope effects on the critical parameters [8,9,28]. There is one report [29] on the IE on CST for the ethylene glycol/nitromethane system, but there is no information on the critical exponent.

Amongst the attempts to explain isotope effects on CST is Guggenheim's derivation of the regular solution model [30]. In this, the CST is directly proportional to the interchange energy between 2 molecules A and B in the pseudo–lattice of the solution. This implies that substitution of molecule B by a lighter isotope B' instead of B will lower the CST due to the smaller interchange en-

ergy. There is no experimental verification for this prediction [27] and such a simple theory involving only lattice vibrations does not work. The effect of the interaction on the internal vibrations of the molecules must also be taken into account. Changes in the location of the critical temperature of a system due to changes in the isotopic composition of one of the constituents should help us in understanding the mechanism by which the intermolecular potential determines the location of the critical point. This is possible, since within the Born Oppenheimer approximation, the electronic potential energy surface is mass independent. A modern theory of isotope effects in condensed phases (CPIE) does exist [31] but has not been applied in detail to critical phenomena, possibly due to lack of sufficient experimental data. Accurate measurements of isotope effects for varied binary systems will contribute towards understanding these effects and facilitate the formulation of a quantitative theory.

1.3 Isotope Effects on PVT Properties

There is a great deal of interest in the study of condensed phase isotope effects (CPIE's). The sign and the magnitude of CPIE'S are closely related to the nature of the intermolecular forces. As stated previously, within the framework of the Born–Oppenheimer approximation, isotope effects (IE) are nuclear mass effects resulting from the motion of different mass nuclei on the same (isotope independent) potential energy surface. A relatively detailed description

of any process of chemical interest, involves formulation of equations of motion on a P.E. surface describing the process. An isotope effect develops because even though the P.E. parameters are mass independent the kinetic energy parameters are not. Thus when the K.E parameters are known in terms of the molecular structure, information on the P.E. surface can be deduced from experimental isotope effects. Isotopic molecules in the liquid and solid state have small but definite differences in the physical properties such as vapor pressure, molar volume, compressibility, transition temperature, etc. Condensed phase isotope effect studies are made for the purpose of enhancing the understanding of the nature of intermolecular forces and of the motions of molecules in condensed phases. Our results will also be useful in refining current ideas about isotope effects on molar volumes [32,33,34,35], compressibility [33], and expansivity [36]. They will be valuable towards formulating a proper theoretical understanding of condensed phase isotope effects [32].

1.3.1 Vapor Pressure Isotope Effects (VPIE)

Of the various IE on thermodynamic properties which have been studied, the IE on vapor pressure has drawn the most attention. This is true not only because the VPIE was historically the first kind of IE on physical properties to be studied but also because it usually shows the largest relative effects. Also it is very simply related to free energy ratios and the data can be used rather directly to test various theories concerning the nature of the condensed state.

The VPIE are of practical interest because they can be capitalised into isotope separation processes.

A complete theory of the VPIE has been presented by Bigeleisen [37]. This theory which was later reviewed by Jancso and Van Hook [31] predicts that the main contributions to the IE result from the vibrational energies of the lattice motions. One can calculate the reduced partition function ratios of isotopic isomers and thus deduce the isotope effects on various thermodynamic properties. The details of the relation of the VPIE to condensed phase molecular properties, molecular structure and vibrational dynamics have been discussed by Van Hook [31]. The VPIE is given by

$$\ln P'/P = \ln(\bar{Q}'_v \bar{Q}_c / \bar{Q}_v \bar{Q}'_c) + 1/RT[(P'V' - PV) - (B'P' - BP)] \qquad (1.7)$$

where the logarithmic pressure ratio $\ln(P'/P)$ refers to a comparison between the pure separated isotopic isomers at a common temperature T, each existing at a different equilibrium volume V' or V, under separate equilibrium vapor pressures P' or P. The prime refers to the lighter isotope. $\ln(\bar{Q})$ is the average molecular partition function for the condensed (c) and vapor (v) phases. The correction terms $(P'V' - PV)/RT$ and $(BP - B'P')/RT$ account for the effect of the difference between Helmholtz and Gibbs free energies of the condensed phase, and for gas imperfection respectively.

If the potential energy surfaces in both vapor and condensed phases are identical for the two isotopic isomers, Bigeleisen [37] has shown that the Q ratio in Eq. 1.7 is equivalent to the ratio of reduced partition functions (RPFR) in

the two phases [38].

$$(s/s')f_i = (\bar{Q}/\bar{Q}')_{qm}/(\bar{Q}/\bar{Q}')_{cl} \tag{1.8}$$

where, Q_{qm} is the quantum mechanical partition function,*i.e.*, for harmonic vibration it is

$$Q_{vitqm} = \prod_{i=1}^{3n-6} \frac{\exp(-u_i/2)}{1 - exp(-u_i)}. \tag{1.9}$$

and in Eqn. 1.8 Q_{cl} is the classical partition function for vibration

$$Q_{clqm} = \prod_{i=1}^{3n-6} 1/u_i \tag{1.10}$$

where $u_i = hc\nu_i/kT$. s and s' are the symmetry numbers of the two isotopic analogs. So,

$$\ln(P'/P) = \ln(f_c/f_g) + 1/RT[(P'V' - PV) - (B'P' - BP)] \tag{1.11}$$

It is often assumed that when the condensed phases coexist at equal temperatures, each under it's own vapor pressure and at it's equilibrium molar volume, the substitution leading to Eqn. 1.11 is proper. However if the ratio of condensed phase volumes V/V', is not equal to the ratio of congruent volumes $V^*/V^{*\prime}$, a correction must be applied to Eqn. 1.11

$$\begin{aligned} \ln(P'/P) \;=\; & \ln(f_c/f_g) + 1/RT[(P'V' - PV) - \\ & (B'P' - BP)] + 1/RT \int_{V'}^{V^*} d(\ln Q'/dV)dV \end{aligned} \tag{1.12}$$

where the term involving the integral corrects the reduced partition function to the congruent state $(Q(T, V = V^*, n)/Q'(T, V'^*, n))$ from the noncongruent

$(Q(T, V = V^*, n)/Q'(T, V', n)$. For congruent fluids $< \nabla^2 U >=< \nabla^2 U' >$, U being the intermolecular potential and $< \nabla^2 U >$ the laplacian of U. For pairwise additivity and spherical symmetry

$$< \nabla^2 U >= 4\pi N \int_0^\infty g(r) d/dr(r^2 d\phi(r)/dr) dr$$

Van Hook [32] has shown $V^* = V - \Delta V(exp)$, $\Delta V(exp)$ being the contribition of thermal expansivity to the isotope effect on the molar volume.

Numerical evaluation of Eqn. 1.12 implies that a self consistent set of $3N$ condensed phase and $3N - 6$ vapor phase frequencies for both members of the isotopic pair are available. These are best obtained by calculation from the known molecular geometry, masses and mass distributions using independent force fields consistent with the spectroscopically observed gas phase frequencies and frequency shifts on condensation. Directly observed frequencies and frequency shifts should not be substituted in the above equation since spectroscopic experimental errors tend to accumulate and this can result in large errors in the calculated VPIE'S. The recommended [31,39] and now standard procedure is based on the FG matrix approach [40].

Detailed calculations of the kind refered to above are extremely tedious, if not impossible without the aid of a digital computer. Consequently it is useful to have an approximate relation for the VPIE estimation for cases where there is not enough input information to define the complete problem. One most common approximation makes use of the fact that very often the 3N molecular frequencies happen to fall into two groups; the first contains the high frequencies

$u_i = hc\nu_i/kT >> 1$ and the second group contains only the low frequencies. This leads to the approximate equation known as the AB equation

$$\ln(P'/P) = A/T^2 - B/T \tag{1.13}$$

which will be useful later. $\ln(P'/P)$ is the VPIE, T is the absolute temperature, and the A and B factors describe the contributions of the external and internal frequencies respectively [41,42]. The low–frequency group contains the external gas–phase frequencies together with corresponding condensed phase values, and can be treated in the first order quantum approximation *i.e.*,

$$A \simeq 1/24 \sum^{ext} (\mu'^2 - \mu^2);\ \mu = h\nu/kT. \tag{1.14}$$

The "large" internal frequencies are treated in the low temperature (zero point energy) approximation because the excitation factors for these frequencies all approach unity. This group contains only internal modes.

$$B \simeq 1/2 \left[\sum^{int} (\mu' - \mu)_g - \sum^{int} (\mu' - \mu)_c \right] \tag{1.15}$$

where g and c denote the vapor and condensed phase respectively.

The A term is always positive and predicts a normal VPIE. The B term arises from intermolecular interaction which causes changes in the various internal force constants. An increase in a given force constant on condensation will lead in the direction of a normal isotope effect, and a decrease will lead to an inverse effect. Practically speaking, Eqn. 1.13 is most useful in fitting VPIE data parametrically. At low enough temperature A/T^2 must predominate; the isotope

effect will be normal and fall off as $1/T^2$. At intermediate temperatures the B term which can be positive, negative or zero, can dominate and may account for a crossover to an inverse isotope effect. Thus the temperature dependence of VPIE can be complicated.

1.3.2 Origin of the Molar Volume Isotope Effect (MVIE)

Recent papers from this laboratory have emphasized the importance of the detailed knowledge of isotope effects on the volumetric properties of fluids including molar volume isotope effects (MVIE's), compressibilities and expansivities, in formulating a proper theoretical understanding of condensed phase isotope effects [33,34,36]. The energy and the free energy of the liquid (and therefore the position and shape of the potential surface) are sensitive functions of condensed phase molar volume or pressure. Because volume is a function of temperature, pressure, and isotopic substitution it is important to understand the origins of the MVIE. An early discussion was given by Bartell and Roskos [43]. They used a mechanical oscillator model and showed that the net isotope effect is a sum of contributions due to isotopic differences in mean square amplitudes of internal vibrations, and contributions from intermolecular (hindered translational) modes. In their model the MVIE does not vary with temperature. However, experiments on benzene, methane, acetone, and methanol show a significant decrease as temperature increases and in fact at high enough temperature, there are inversions of sign to give inverse isotope effects, which become large as the

critical temperature is approached [33,36,44,45].

It has been suggested [46,35] that the temperature dependence of the MVIE can be understood by using a model which includes the steric and the lattice effects, but which also takes into account the second order effect introduced by thermal expansion. This approach, though providing a coherent model for the MVIE of liquids at low temperatures and pressures (*.i.e.,* near the triple point), has not been treated completely and no specific conclusions have been drawn. Thus, it seems that the present understanding of the MVIE is still at the "beginners" level, along with the isotope effects on compressibility and expansivity which have also not been quantitatively formulated.

There is a continuing interest in the measurement of isotope effects on various compounds and solutions at the University of Tennessee. Measurements of isothermal compressibilities and expansivities in solutions of benzene, cyclohexane and their isotopic isomers [33] and for methanol and acetone [34,36] have been completed in this laboratory. In the present work we have extended the experimental techniques and theoretical analysis to measurements of vapor pressure, isothermal compressibilities, expansivities and molar volumes for ethylene glycol and D–ethylene glycol for temperatures between $373K$ and $573K$. Vapor pressures for ethylene glycol have previously been reported for temperatures from $373K$ to $493°K$ [47,48,49,50,51,52,53]. The MVIE is reported at 20 and $70°C$ [54]. There is no previous literature on the isotopic differences in isothermal compressibilities and expansivities of ethylene glycol.

CHAPTER 2

Experimental

This chapter is divided in two sections. Section 2.1 deals with the description of the experiment to measure the pressure dependence and isotope effect on critical demixing of the ethylene glycol/nitromethane binary system. Section 2.2 deals with the experiment for vapor pressure, molar volume and compressibility measurements.

2.1 CST Measurements

This section is divided into subsections dealing with the details of materials and instrumentation used for measurements of the critical parameters describing the coexistence curve.

2.1.1 Choice of System

A liquid–liquid binary system can be studied with high precision if it has an experimentally convenient CST. Several systems have been studied whose CST at atmospheric pressure is between 25 and 60°C. CST measurements are extremely sensitive to impurities [16,55,17,18,19]. Hence, ease of purification of the materials used also becomes an important requirement. The CST for the ethy-

lene glycol–nitromethane system lies at $37°C$ at atmospheric pressure. The two components can be purified and dried with relative ease. This system has an additional advantage in that the densities of the two components are close enough that the possible errors in CST measurements due to gravitational gradients are reduced.

2.1.2 Materials

Analytical grade nitromethane was obtained from Mallinckrodt. It was first dried over anhydrous $CaCl_2$ and then distilled twice, with a high reflux ratio in a 1.2 meter long Nester Faust spinning–band distillation column. The distillation was carried out at 300 *torr* in order to keep the pot temperature below $70°C$.This is necessary because some decomposition is expected above $90°C$. The first and last portions were discarded.

Ethylene glycol obtained from Mallinckrodt was dried over molecular sieves and distilled in the spiral rotating column at a reduced pressure of 120 *torr* with the pot temperature at $135°C$. The molecular sieves were previously heated at $350°C$ for three days or more.

Deuterated ethylene glycol $(CH_2OD)_2$ was prepared by refluxing reagent grade 99.8% D_2O and ethylene glycol in the ratio 2.5 moles D_2O : 1 mole glycol and removing the water by fractional distillation at a reduced pressure of 100 *torr*. The water fraction boiled off at $60°C$ and the deuterated glycol fraction was collected at $120°C$. This fraction was dried over molecular sieves

and redistilled to remove any traces of moisture. NMR showed 98.0% ± 0.1%D content.

The densities of ethylene glycol and deutero ethylene glycol were found to be $1107.5 Kg/m^3$ and $1136.76 Kg/m^3$ respectively. The densities were measured using a Mettlar–Paar DMA 60 vibrating tube densitometer.

2.1.3 Experimental Setup

The CST apparatus is shown in Fig. 2.1 It consists of a high pressure stainless steel cell thermosttated in a silicone oil bath, a stainless screw injector for pressure generation, and the pressure, temperature and phase transition metering instruments.

The cylindrical high pressure cell is $5in$ long and $3in$ in diameter. It has a thermowell which contains an 100 ohm platinum resistance thermometer. The cell is fitted with sapphire windows at either end. A $(1/8)^{"}$ stainless steel tube is silver soldered at the bottom of the cell and used to fill, empty, and pressurize the cell. There is a small well at the bottom of the cell to contain a teflon coated magnetic stirring bar.

The cell is connected to the screw injector (SI) and the pressure gage with $1/8^{"}$ stainless steel tubing and high pressure stainless valves. The entire apparatus is connected to a vaccum line that is pumped through a liquid nitrogen trap by a rotary oil pump and an oil diffusion pump. The sample mixture is stored in a $50ml$ glass sample vessel connected to the vaccum line by flexible stainless

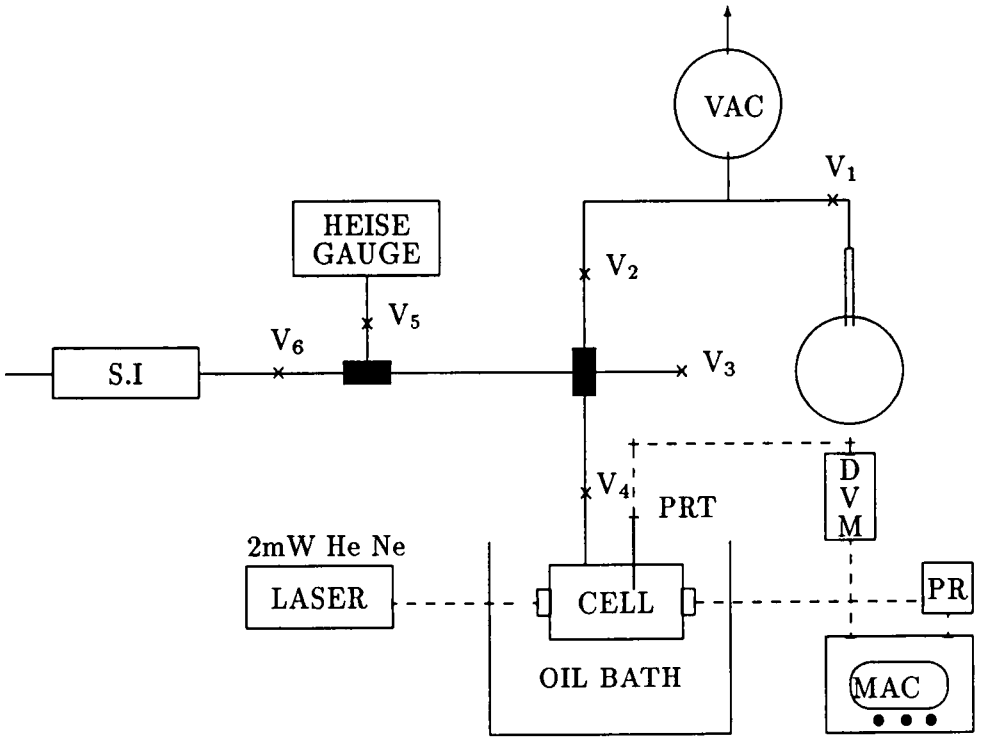


Figure 2.1: Critical solution temperature apparatus. PR – Photo resistor (2 to 150 Kohms); PRT – Platinum resistance thermometer; MAC – Apple II+ computer

tubing. The cell is placed in a bath filled with silicone oil. The temperature of the bath is controlled by a Lauda K4/R bath , which pumps thermostatted water through copper coils placed in the bath. The bath and the flow tubes are very well insulated and the bath temperature is controlled to within $\pm 0.001K$.

The pressure generator is a stainless screw injector (HIP) of volume $20cm^3$ and maximum pressure of 200 MPa. The screw injector is connected to a Heise pressure gauge (model # 711A) and to the cell by $(1/8)^{"}$ stainless steel tubing.

The temperature is measured by a 100 ohm, 4 lead platinum resistance thermometer. The calibration of this thermometer is available elsewhere[1]. The resistance is measured to 0.0001 ohms by a microprocessor controlled digital voltmeter, yielding a precision of $0.2mK$ in the temperature measurements.

2.1.4 Detection of Phase Transition

One of the more striking manifestations of the critical point is the scattering of light, a phenomenon known as critical opalescence. A sharp beam of light from a $3mW$ HeNe laser is passed through the sample cell. While the two liquids are completely mixed the beam emerging out of the cell is a sharp pinpoint. As the two phases separate at the critical point the emerging beam becomes very diffused over a temperature range of $10mK$. This enabled Singh [56] to automate the entire procedure by placing an EG and G type VT–701 photoresistor in the

[1]see appendix

beam path. The photoresistor is wired to an Apple II+[2] computer which reads the resistance of the photoresistor. These signals are then transformed such that the computer assigns integer values from 1 to 100 as the intensity changes from bright to dim. The point at which the intensity becomes one half the original is taken as the phase separation temperature.

2.1.5 Data Acquisition

As stated above the data acquisition process is automated. The transition is detected by laser light scattering. The temperature is measured by the platinum thermometer whose output is available on a RS232c interface. This output is read by a suitably programmed Mountain Computer CPS card which is also plugged into the Apple computer. The pressure is read by a Heise pressure gage whose output is sampled by a DI09 parallel interface card also plugged into the computer.

The temperature, pressure, and light intensity data is monitored every 6 seconds. When a transition occurs, the computer records the data at and in the vicinity of the transition point, heats the bath to a preset temperature, and repeats the data acquisition for a preprogrammed number of times.

[2]Apple II+ is a trademark of Apple Computers, Inc.

2.1.6 Experimental Procedure

All the binary mixtures for CST measurements were prepared very carefully by gravimetric methods. The samples were degassed thoroughly by several freeze–pump–thaw cycles, with a pumping pressure of 1×10^{-1} Pa or less. In a typical run, the bath, the connecting tubes and the screw injector are all heated to at least 3 to $4K$ above the expected phase transition temperature. Then the sample mixture is warmed until it completely mixes and the mixture is allowed to flow into the previously heated and evacuated sample cell and screw injector. The liquid is drawn into the system while the screw injector is opened very slowly to ensure that no gaps are created. Valve V_2 is then closed and the pressure applied by pushing down on the screw injector. Valve V_3 remains closed all the time.

The bath temperature is then allowed to cool down to the phase transition temperature at a cooling rate of 3–5 mK per minute. The operating computer program collects the pertinent data for a preset number of runs. The pressure is changed manually and the procedure is repeated.

2.2 Vapor Pressure, Molar Volume, and Compressibility Measurements

This section describes the apparatus and experimental procedures used for the study of vapor pressure, molar volume, compressibility and their isotope

effects in ethylene glycol.

2.2.1 Apparatus

This experiment involves a differential comparison of two pure liquids or solutions contained in a common thermostat at a common temperature [34]. The total pressure of the more common isotope is also measured, along with the isotopic pressure difference at a temperature T.

The apparatus is shown in Fig. 2.2. It consists of the following:

1. Two precision machined stainless steel screw injectors (SI) (HIP Engineering) of volume about $30cm^3$. The screw injectors have been calibrated such that the amount of material pushed from the screw injector into the sample cells and the pressurizing network can be obtained within $\pm 0.001cm^3$.

2. Two similar stainless steel cylindrical sample vessels (V_1 and V_2) each of volume about $25cm^3$ are fitted in a large copper block which is hung in a Hart 5005 thermostatic bath. This ensures that both the isotopic samples are at exactly the same temperature at all times. The thermostatting liquid is Dow Corning 210H silicone oil. The bath and the block are both fitted with platinum resistance thermometers that are read with a Keithly 705 scanner and 195A multimeter. These thermometers are calibrated against a standard platinum thermometer certified against IPTS–68 and traceble to NBS. The calibration data and the least squares fits for the

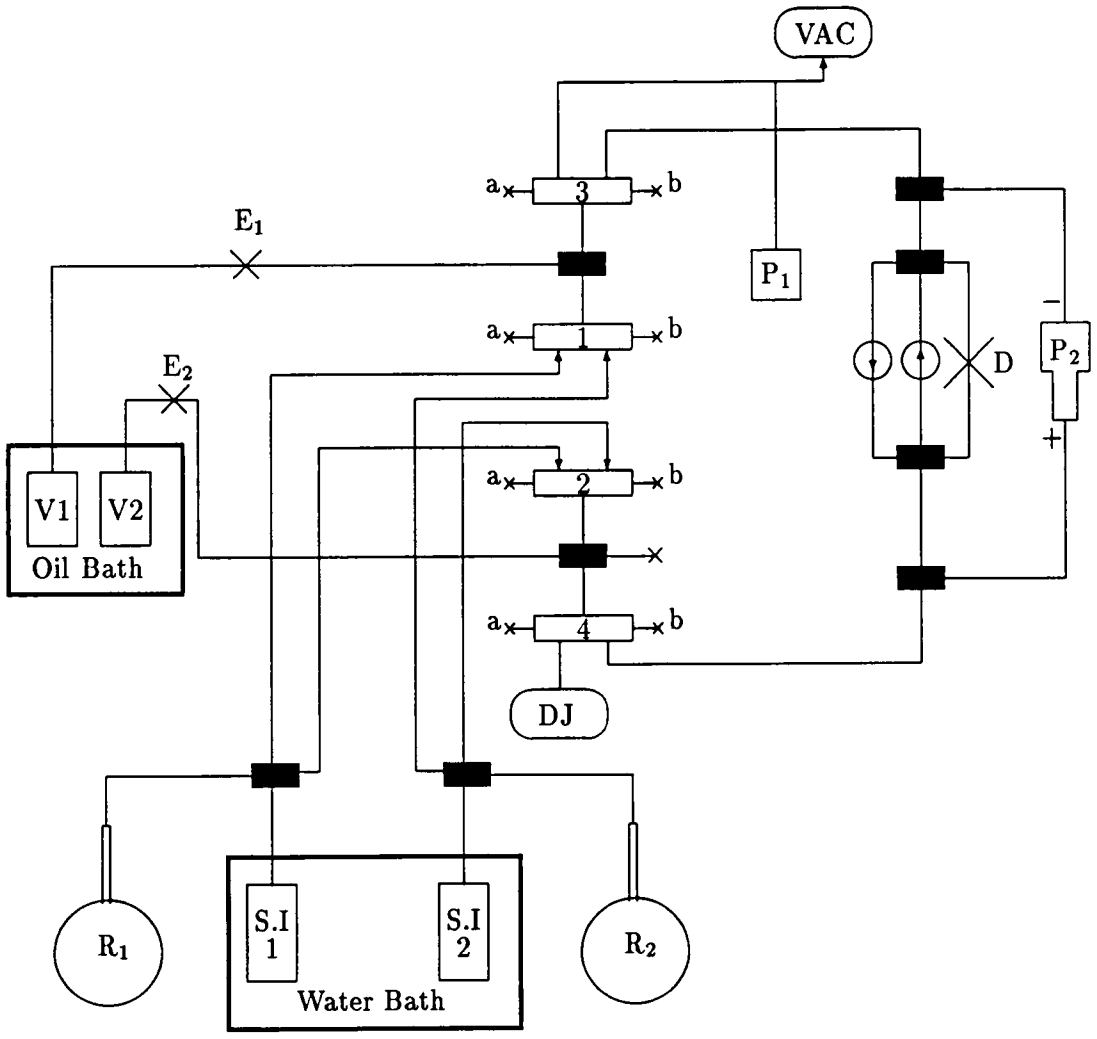


Figure 2.2: P–V–T Apparatus

non–linear function describing the temperature–resistance relationship for the block thermometer is given in Appendix 1. The temperature of the bath is steady to $\pm 1mK$ or better, over the range from room temperature to $300°C$. The temperature differences between samples during an experiment is estimated to be 0.1 mK or less.

3. The absolute pressure of the liquid in one cell (usually the lighter isotope), and the differential pressure between two liquids in two cells are measured by quartz oscillator "zero" displacement transducers (Paroscientific, Redmond, WA, rated precision 0.01% of full scale, 60 and 1.4 bars respectively).

4. Valve manifold: The screw injectors,the sample cells, and the pressure transducers are all connected by 1.6 mm diameter stainless capillary lines and stainless high pressure 2–way and 3–way valves. The arrangement of the valves is such that the two samples can be completely isolated from one another. There are however, two checkvalves which open and allow the two fluids to flow into one another, if the pressure difference between them becomes close to $\pm 20psi$, this being the upper limit of the differential pressure transducer. The valve manifold and the pressure transducers are enclosed in a wooden box. This airbath is thermostatted by circulating water from a Lauda C–12 bath, through copper coils fixed to the inside of the box. The screw injectors are thermostatted in a well insulated water

bath. The airbath and the water bath are maintained close to $30°C$ during the experiment.

2.2.2 Experimental Procedure

The entire apparatus is pumped through a glass vaccum line by a mercury diffusion pump and a rotary oil pump. The apparatus and the samples are degassed thoroughly using at least five freeze–pump–thaw cycles with a pumping pressure of 1×10^{-3} Pa or less. Any traces of air in the system would yield errors of large magnitude in the vapor pressure amd compressibility measurements. Ethylene glycol and deuterated ethylene glycol are drawn into SI(1) and SI(2) from glass sample flasks R_1 and R_2 while keeping valves 1A and 1B closed. The lighter isotope is then allowed to flow into the absolute pressure gage and into the differential pressure gage by opening valves 1A and 3A. the middle valve D is kept open at this time. Valve 2B and 4B are then opened and the other isotope B is pushed into the lines till valve E2 and into the differential pressure line where an interface of the two liquids is formed. The middle valve D is now closed.

For vapor pressure measurements, valves E1 and E2 are opened and the two cells are filled two–thirds with the two liquids. The absolute pressure of one isotope and the vapor pressure difference between the two isotopes are measured simultaneously for different temperatures from $30°C$ to $300°C$ at an interval of 10 to $15°C$. Care is taken to see that the absolute pressure does not exceed the

maximum gauge pressure of 6 MPa.

In the molar volume measurements, the liquid is forced from the screw injectors into the cells while monitoring the amount of liquid introduced and the corresponding pressure. Once the condensation pressure is reached the cell fills at the sample vapor pressure. At this point, the pressure jumps abruptly when additional liquid is forced into the cell. The intersection of the flat and the steep portion of this (n, P) defines the liquid phase molar volume at equilibrium vapor pressure. Compressibility is then determined by continued injection of the liquid until the maximum gage pressure is reached. The molar volumes and compressibilities of the two isotopes were measured individually at similar temperatures. The precision of this experiment is determined by $\delta n/n$ and is calculated to be one in ten thousand.

CHAPTER 3

Experimental Results

This chapter consists of three sections. Vapor pressure measurements and their isotope effects are given in section 3.1. Section 3.2 deals with molar volume, expansivity, compressibility and their isotope effects. The results of the studies of the co–existence curve for $(CH_2OH)_2 + CH_3NO_2$ are given in section 3.3.

3.1 Vapor Pressure

Absolute vapor pressure for the H isotope and the differential vapor pressure $P' - P$ were measured from 373 to $574K$ at intervals of 5–$10K$. The $'$ refers to the lighter isotope. The vapor pressure of ethylene glycol below $373K$ is small and not conveniently measured with our apparatus. The absolute vapor pressure of deuterated ethylene glycol was calculated from the differential pressure and the value of P' obtained from absolute pressure measurements. The experimental data expressed as P' and $P' - P$ is given in Table 3.1. Plots of $\ln P'$ vs T and $\ln P$ vs T are seen in Fig. 3.1 and Fig. 3.2 respectively.

The vapor pressure data were fitted to the following three equations in order

Table 3.1: Vapor pressure data for $(CH_2OH)_2/(CH_2OD)_2$

#	T/K	P_H/MPa	$\Delta P \times 10^4$/MPa
1	374.041	0.0022	1.22
2	380.113	0.0029	1.436
3	383.203	0.0035	1.64
4	387.746	0.0044	1.912
5	392.335	0.0055	2.169
6	397.793	0.0071	2.541
7	402.876	0.0089	3.042
8	410.413	0.0123	3.656
9	415.327	0.0149	4.37
10	423.582	0.0206	5.554
11	433.869	0.0308	7.407
12	444.559	0.0447	10.23
13	450.307	0.0531	11.3
14	454.382	0.0612	12.66
15	463.631	0.0827	16.48
16	470.856	0.1035	18.78
17	476.279	0.1219	21.5
18	480.763	0.1389	25.19
19	486.083	0.1615	28.79
20	491.140	0.1846	32.19
21	495.436	0.2077	35.82
22	505.817	0.2692	45.41
23	525.255	0.4272	67.76
24	534.361	0.517	81.05
25	545.831	0.6628	104.5
26	554.229	0.8045	121.3
27	563.314	0.9466	134.9
28	570.303	1.0912	157.1

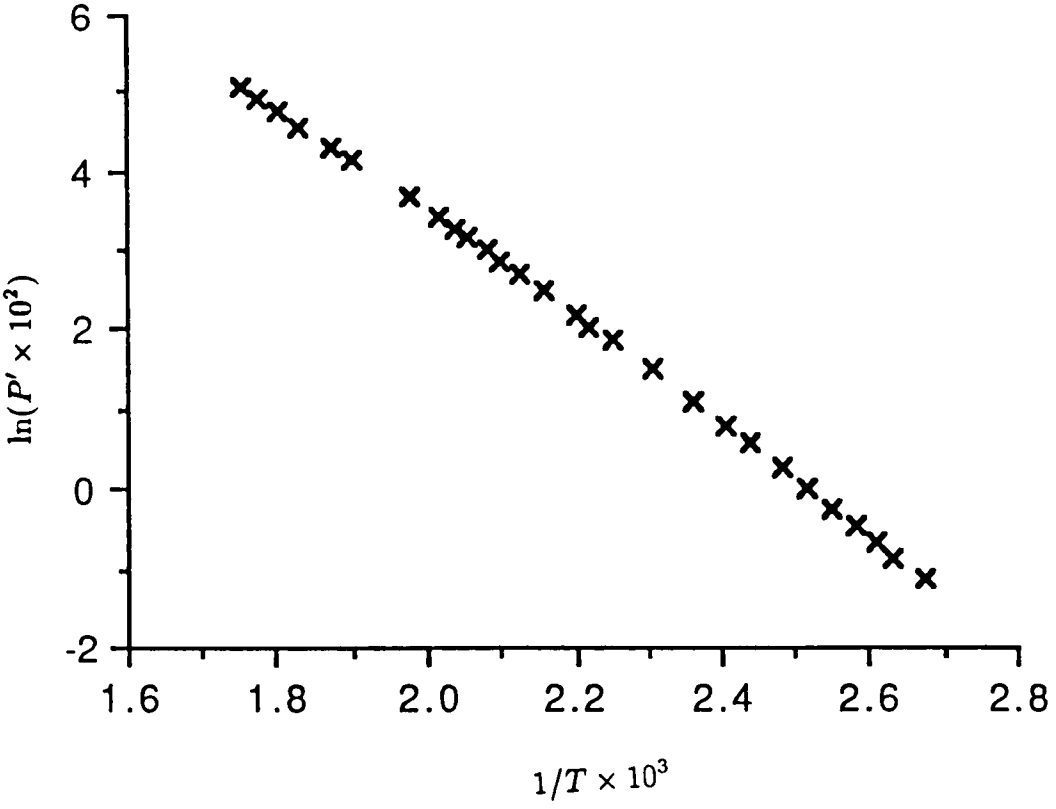


Figure 3.1: Plot of $\ln P'$ vs $1/T$

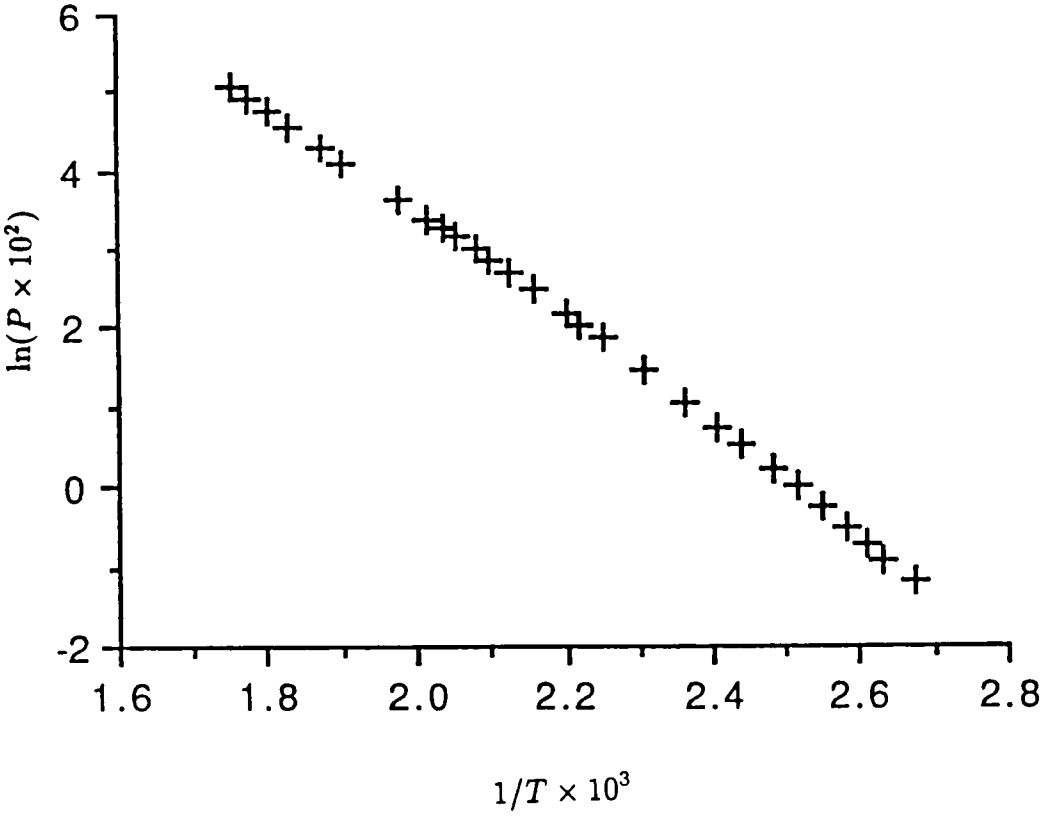


Figure 3.2: Plot of $\ln P$ vs $1/T$

to find the one that would best represent the data.

$$\ln P = A/T + B + CT + DT^2 \quad (300 < T/K < 575) \tag{3.1}$$

$$\ln P = \frac{A}{(T+B)} + C \tag{3.2}$$

$$T/K \log(P) = \frac{a_0}{2} + \sum_{s=1}^{3} a_s E_s(x) \tag{3.3}$$

where, P is the pressure; $E_s(x)$ is the Chebyshev polynomial in x of degree s and $x = 2T - (T_{max} + T_{min})/(T_{max} - T_{min})$.

Equation 3.1 is a form of the thermodynamically based Nernst equation. Equation 3.2 is the Antoine equation and Eqn. 3.3 is the Chebyshev polynomial. Various data found in the literature were also fit to these equations. The parameters obtained from the fits of our data and the literature data and the variances of the fits are given in Tables 3.2, 3.3, 3.4. For further work we have represented our data by the following Eqn. since the deviations $\delta \ln P = \ln P_{calc} - \ln P_{expt}$ are small

$$\ln P^{0'} = \frac{(-10389.97 \pm 434)}{T} + (34.74 \pm 2.82) + (-0.0365 \pm 0.006)T + (2.064 \pm 0.43) \times 10^{-5} T^2 \quad (373 < T/K < 574) \tag{3.4}$$

$$\sigma^2 = variance = 5.08 \times 10^{-5}.$$

Figure 3.3 is a deviation plot that compares the present $(CH_2OH)_2$ data (Table 3.4) with the Ambrose [47] ($373 < T/K < 496$), TRC tables [53] ($373 < T/K < 473$), and the Stull [50] data ($373 < T/K < 473$).

Table 3.2: Equation (1) parameters

Ref.	A(K)	B	C(K^{-1})	10^5.D(K^{-2})	σ^2
SVH	-10389.97 ± 434	34.74 ± 2.82	-0.0365 ± 0.006	2.064 ± 0.43	5.08×10^{-5}
Ambrose	-9759.53 ± 49	30.83 ± 0.34	-0.0283 ± 0.0005	1.476 ± 0.062	8×10^{-8}
Taylor (1926)	-5509.78 ± 1138	8.68 ± 5.38	0.0064 ± 0.0006		2.46×10^{-3}
$(CH_2OD)_2$	-11892.37 ± 614	43.57 ± 4	-0.54 ± 0.008	3.22 ± 0.61	1.11×10^{-4}
Stull	-6889.75 ± 120	14.15 ± 0.62	0.0011 ± 0.0007		1.43×10^{-4}

Table 3.3: Antoine equation parameters

Ref.	A	B	C	σ^2
SVH	11.381 ± 0.063	-4328.6 ± 46	-89.424 ± 1.93	4.89×10^{-5}
Ambrose	11.44 ± 0.021	-4409.23 ± 14	-84.95 ± 0.56	1.25×10^{-6}
TRC	13.43 ± 0.15	-5877.55 ± 116	240.59 ± 3.85	3.31×10^{-5}
$(CH_2OD)_2$	11.095 ± 0.084	-4109.69 ± 59.33	-100.77 ± 2.49	1.079×10^{-4}

Table 3.4: Parameters for the Chebyshev polynomial

Ref.	A_0	A_1	A_2	A_3
SVH	1415.18 ± 1.26	22.94 ± 1.52	-36.37 ± 1.00	5.16 ± 1.07
Ambrose	1289.42	508.28	-7.37	0.356

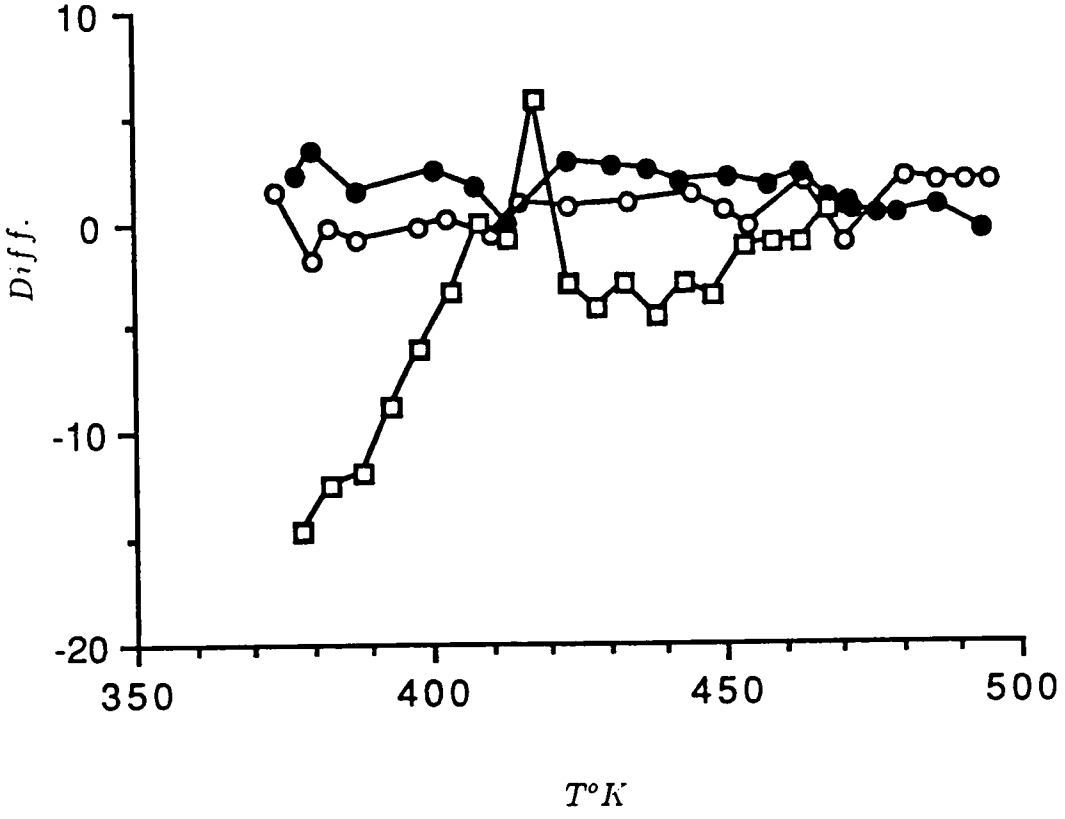


Figure 3.3: Deviation plots for vapor pressure of $(CH_2OH)_2$: ○ $\ln P_{This\ work} - \ln P_{\text{Ambrose}}$; • $\ln P_{This\ work} - \ln P_{\text{TRC}}$; □ $\ln P_{This\ work} - \ln P_{\text{Stull}}$

The present $(CH_2OH)_2$ data agree best with the Ambrose data ($\delta \ln P < 1\%$) in the temperature range $373 < T/K < 473$. The Stull values were obtained from graphical smoothing and the form of the present plot is somewhat too sensitive for them. The TRC values were obtained from an Antoine equation. The Schierholtz and Staples [48] data report one of the earliest measurements on the vapor pressure of ethylene glycol and are represented with two simple $1/T$ equations which appear discontinous in a curve of the above type. They are therefore not considered any further. The values of Jones and Tamplin [51] were derived from an Antoine Equation, but there has been unwarranted smoothing and their tabular points are fairly widely scattered and hence fall much below the curve shown.

The data for the absolute vapor pressures of $(CH_2OD)_2$ were also fit to Eqn. 3.1 to yield

$$\begin{aligned} \ln P^o &= \frac{(-11892.38 \pm 614)}{T} + (43.57 \pm 4.0) + (-0.054 \pm 0.008)T + \\ &\quad (3.22 \pm 0.61) \times 10^{-5} T^2 \quad (373 < T/K < 574). \qquad (3.5) \\ \sigma^2 &= \textit{variance} = 1.11 \times 10^{-4}. \end{aligned}$$

There is no prior literature data for comparison.

3.1.1 Vapor Pressure Isotope Effects (VPIE)

The VPIE is reported in terms of the AB Eqn. 1.13. The VPIE data is given in Table 3.5 and is plotted in Fig. 3.4. Least squares representation of all the

Table 3.5: VPIE for $(CH_2OH)_2/(CH_2OD)_2$

#	T/K	$10^2 \ln(P_H/P_D)$
1	374.041	5.68
2	380.114	5.026
3	383.203	4.75
4	387.746	4.44
5	392.335	4.025
6	397.793	3.66
7	402.876	3.46
8	410.413	3.02
9	415.327	2.96
10	423.582	2.73
11	433.869	2.428
12	444.559	2.29
13	450.308	2.15
14	454.383	2.09
15	463.631	2.012
16	470.856	1.83
17	476.279	1.78
18	480.763	1.83
19	486.083	1.79
20	491.141	1.76
21	495.436	1.74
22	505.817	1.69
23	525.255	1.59
24	534.361	1.58
25	545.831	1.59
26	554.229	1.51
27	563.314	1.45
28	570.303	1.45

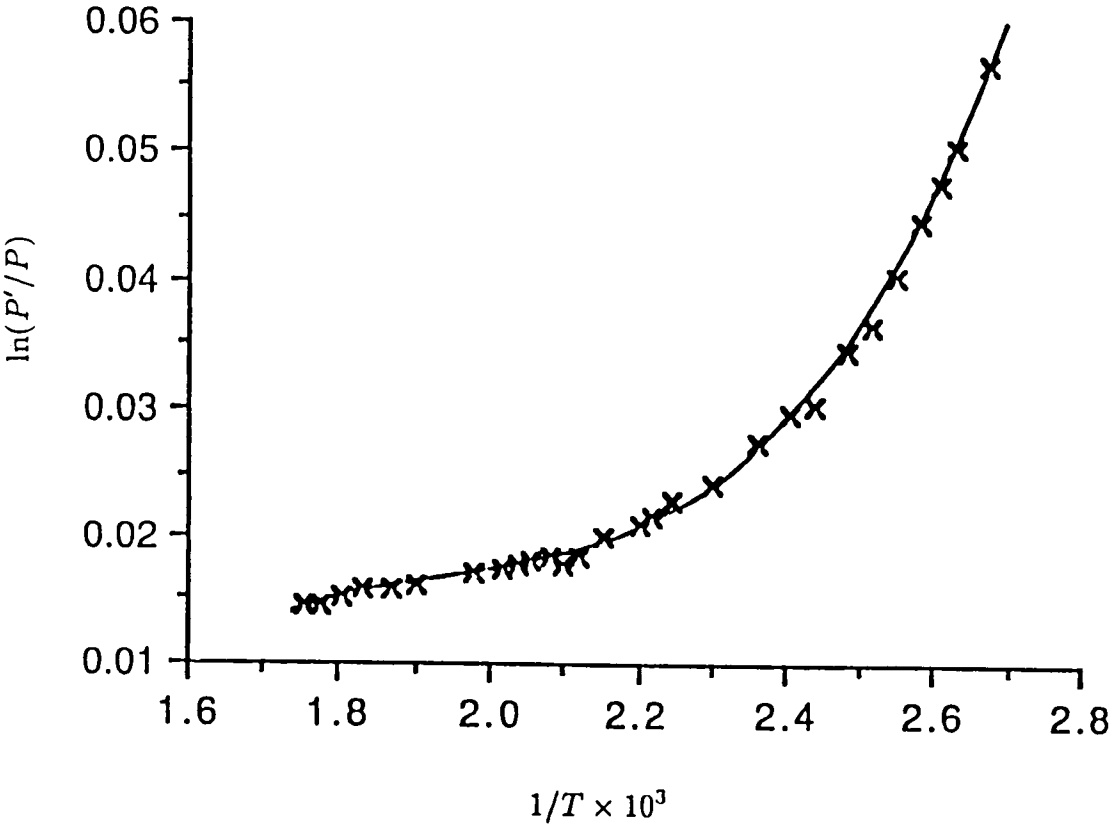


Figure 3.4: Plot of $\ln(P'/P)$ vs $1/T$

data points yields

$$\ln\left(\frac{P^{0\prime}}{P^0}\right) = \frac{13649.77 \pm 1365.75}{T^2} - \frac{18.97 \pm 3.12}{T} \qquad (3.6)$$
$$\sigma^2 = variance = 1.94 \times 10^{-5}.$$

We have generated a second least–squares fit of the form

$$\ln\left(\frac{P^{0\prime}}{P^0}\right) = (0.2655 \pm 0.0257) - \frac{(261.17 \pm 23.49)}{T} + \frac{(68014.48 \pm 5300.09)}{T^2} \quad (373 < T/K < 574) \qquad (3.7)$$
$$\sigma^2 = variance = 3.85 \times 10^{-6}.$$

The magnitude of the VPIE seemed somewhat large at the lower temperatures, so we fit the data above $400K$. This high temperature data fit yields,

$$\ln\left(\frac{P^{0\prime}}{P^0}\right) = (0.1484 \pm 0.1288) - \frac{(147.03 \pm 12.31)}{T} + \frac{(40552.93 \pm 2917.81)}{T^2} \quad (400 < T/K < 574) \qquad (3.8)$$
$$\sigma^2 = variance = 3.9 \times 10^{-7}.$$

The high temperature VPIE is plotted in Fig. 3.5. Equation 3.7 produces a minimum at $526K$ which is not observed experimentally therefore Eqn. 3.6 is preferred since the high temperature behaviour is better represented.

3.2 Molar Volumes, Compressibilities, and Expansivities

Experimental results of the volumetric property measurements are enumerated in this section.

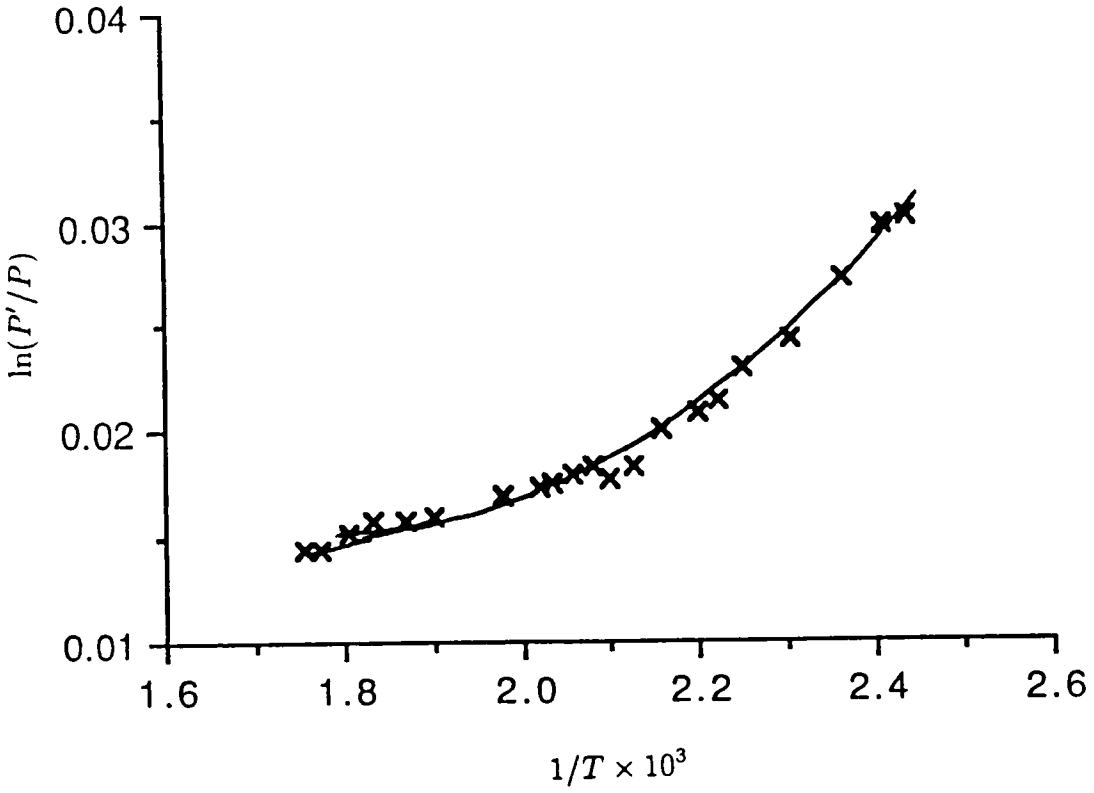


Figure 3.5: VPIE for $T > 400K$

3.2.1 Molar Volumes

Molar volume measurements were carried out in separate runs on the two isotopes keeping temperatures approximately same. Referring to Fig. 2.2 we can see that two valves (E_1 and E_2) separate the screw injectors and their connecting lines from the sample vessels and the lines coming from them. The number of moles on the measuring side of the system (*i.e.*, in the sample cells) is the difference between the number of moles on the SI side at the begining of the experiment (*i.e.*, when E_1 and E_2 are closed and no liquid has yet been injected into the sample side) and the number of moles on the measurement side. The volume in the connecting lines has been measured to be 8.2315 *cc*. The total volume of SI(1) is 30.0345 *cc* and the total number of turns on SI(1) is 84.6. Therefore for every complete turn of the SI, 0.355 *cc* of the liquid are added to the system. The details of these calibrations are given elsewhere [36].

The experiment measures P as a function of SI setting. Volumes were measured by determining $n(s)$ as a function of P from just above the equilibrium pressure to 6 MPa (which was the upper limit on the absolute pressure transducer) at 25° intervals from 303 to 574K. Normally 10–11 data points were obtained for each temperature. Each data set was then fit with the relation

$$\ln V_T(\mathrm{m}^3/\mathrm{mol}) \;=\; \sum_{i=0}^{1} A_i (P - P^0)^i \quad P^0 < P/\mathrm{MPa} < 6. \tag{3.9}$$

P^0 was calculated from Eqn. 3.4 above. Trial fits to a 3 parameter Eqn. $\ln V = A_0 + A_1(P - P^0) + A_2(P - P^0)^2$ did not improve the statistical reli-

ability and are therefore not further considered. The A_i parameters for each isotope at experimental temperature are reported in Table 3.6. The A_0 parameters represent volumes under condition of equilibrium vapor pressure, V_t, P^0 (orthobaric) and the A_1 parameters are the compressibilities $\kappa_t = d\ln V_t/dP$.

Figure 3.6 is a plot of $\ln V_{t,P^0}$ vs T for $(CH_2OH)_2$ and $(CH_2OD)_2$. The temperature dependence is given by

$$\begin{aligned} \ln V'_{t,P^0} &= -9.69562 - 8.1555 \times 10^{-4}T + 1.58609 \times 10^{-6}T^2 \qquad (3.10) \\ \sigma^2 &= variance = 5.8 \times 10^{-5} \end{aligned}$$

$$\begin{aligned} \ln V_{t,P^0} &= -9.88921 - 0.2837 \times 10^{-4}T + 0.95275 \times 10^{-6}T^2 \qquad (3.11) \\ \sigma^2 &= variance = 3.17 \times 10^{-5} \end{aligned}$$

The data reported in Table 3.6 was used to generate sets of isobaric $V'(P', T)$ molar volumes at experimental temperatures starting from $10bars$–$60bars$ at $10bar$ interval and this smooth data was fit to polynomial expressions of the type

$$\ln(V'(P)/\mathrm{m}^3/\mathrm{mol}) = \sum_{i=0}^{2} B_i T^i \quad 300 < T/K < 575K \qquad (3.12)$$

The B_i parameters for $(CH_2OH)_2$ are given in Table 3.7.

3.2.2 Compressibilities

Isothermal compressibilities at the experimental temperatures T_{ex}, can be expressed in terms of the A_i parameters obtained from Eqn. 3.9 and listed in

Table 3.6: Parameters for Eqn. 4: $\ln V_T(\mathrm{m^3/mol}) = \sum_{i=0}^{1} B_i(P - P^0)^i$

$(CH_2OH)_2$				
#	T/K	$-B_0$	$-10^4 B_1$/MPa	$\sigma^2 \times 10^{10}$
1	303.507	9.80228	3.73	2
2	323.196	9.78956	4.03	5
3	348.316	9.78669	4.41	8
4	372.916	9.78326	4.83	3
5	398.919	9.76383	5.10	1
6	424.978	9.74227	6.65	27
7	448.333	9.75050	7.37	6
8	498.222	9.71600	9.99	7
9	522.294	9.68909	12.06	198
10	548.554	9.67058	15.05	268
11	573.187	9.63450	20.05	624
$(CH_2OD)_2$				
1	303.542	9.79705	3.73	12
2	323.160	9.78431	4.38	19
3	348.483	9.76719	4.67	20
4	372.657	9.73503	5.31	88
5	398.369	9.71498	5.37	460
6	423.890	9.70806	6.72	22
7	447.015	9.68666	7.97	175
8	498.105	9.63326	10.28	14
9	522.308	9.63608	12.44	277
10	548.409	9.60164	15.05	45
11	573.388	9.53790	20.90	1720

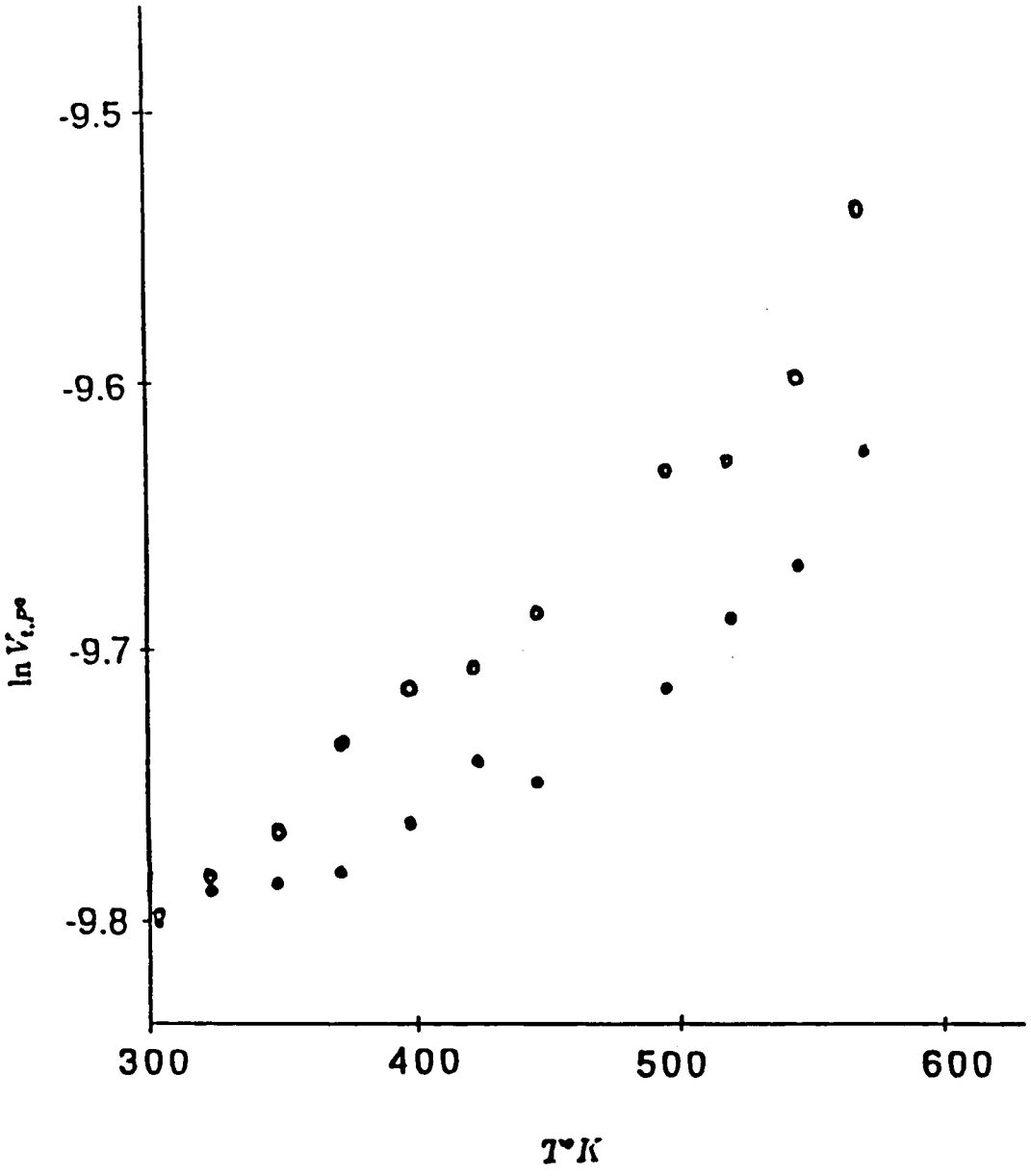


Figure 3.6: Plot of $\ln V_{i,P^o}$ vs T • $(CH_2OH)_2$; o $(CH_2OD)_2$

Table 3.7: Parameters for Equation 3.12

P/MPa	B_0	$10^4 B_1/K$	$10^6 B_2/K^2$
1	−9.72333	−6.8398	1.43873
2	−9.72575	−6.7110	1.41837
3	−9.73041	−6.4712	1.38458
4	−9.73393	−6.2879	1.35765
5	−9.73751	−6.1016	1.33034
6	−9.73487	−6.2291	1.33962
$P^{0'}$	−9.69562	−8.1555	1.58609
P^0	−9.88921	−0.2837	0.95275

Table 3.6. Thus for $(CH_2OH)_2$

$$\kappa'_{(T_ex)} = \sum_{i=1}^{1} -iA'_i(P - P^{0'})^{i-1} = -A'_i \tag{3.13}$$

The temperature dependence of these isothermal compressibilities is

$$\begin{aligned} \ln(\kappa'/\mathrm{MPa}^{-1}) &= -7.481 - 5.224 \times 10^{-3}T + \\ &\quad 1.2875 \times 10^{-5}T^2 \end{aligned} \tag{3.14}$$

$$\sigma^2 = \text{variance} = 1.4 \times 10^{-3}$$

$$\begin{aligned} \ln(\kappa/\mathrm{MPa}^{-1}) &= -7.704 - 3.813 \times 10^{-3}T + \\ &\quad 1.1121 \times 10^{-5}T^2 \end{aligned} \tag{3.15}$$

$$\sigma^2 = \text{variance} = 2.9 \times 10^{-3}$$

The compressibilities for $(CH_2OH)_2$ and $(CH_2OD)_2$ are plotted in Fig. 3.7. $\kappa'(303) = 3.733 \times 10^{-4}\mathrm{MPa}^{-1} \pm 0.001$ and $\kappa(303) = 3.826 \times 10^{-4}\mathrm{MPa}^{-1} \pm 0.002$. Reported values for $(CH_2OH)_2$ are $\kappa'(298) = 3.442 \times 10^{-4}\mathrm{MPa}^{-1}$ [57] and $\kappa'(298) = 3.72 \times 10^{-4}\mathrm{MPa}^{-1}$ [58]. The compressibilities increase with increasing temperature. $\kappa'(378.15) = 4.989 \times 10^{-4}\mathrm{MPa}^{-1}$ as compared to $\kappa'(378.15) = 5.14 \times 10^{-4}\mathrm{MPa}^{-1}$ [58]. From the present experiment $\kappa'(574) = 1.98 \times 10^{-3}\mathrm{MPa}^{-1} \pm 0.001$ and $\kappa(574) = 2.09 \times 10^{-3}\mathrm{MPa}^{-1} \pm 0.002$.

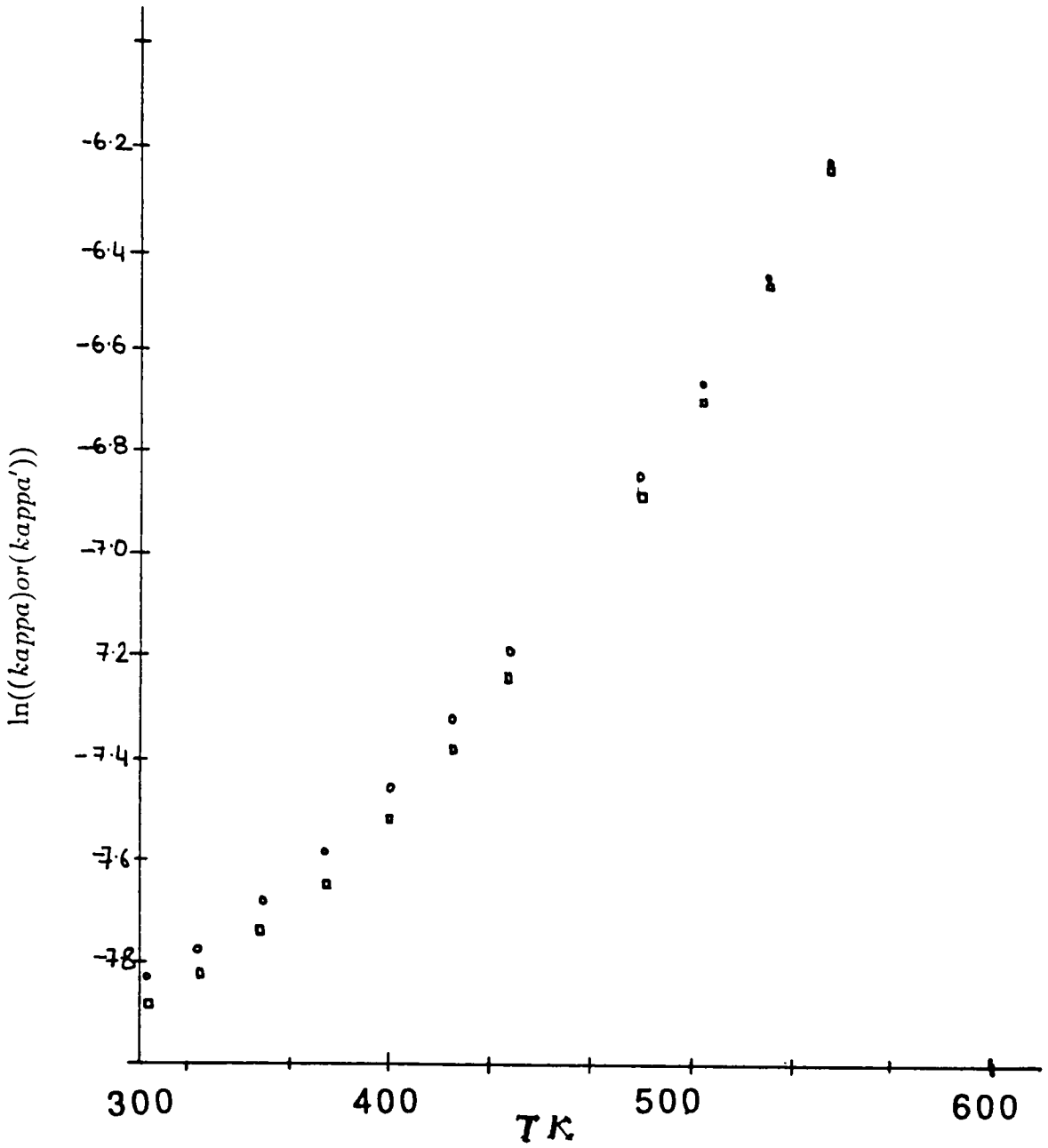


Figure 3.7: Compressibilities for □ $(CH_2OH)_2$; o $(CH_2OD)_2$

3.2.3 Expansivities

The coefficient of thermal expansion for $(CH_2OH)_2$ α', is given by $d\ln V'/dT$. $lnV'(P)$ has been expressed in Eqn. 3.12 as

$$\ln V'(P)/\mathrm{m}^3/\mathrm{mol} = \sum_{i=0}^{2} B_i T^i.$$

α' can therefore be obtained by differentiating Eqn. 3.12 with respect to T to yield the expression

$$\alpha' = \sum_{i=1}^{2} iB_i T^{i-1} \tag{3.16}$$

$$\alpha' = B_1 + 2B_2 T \tag{3.17}$$

Using Eqn. 3.17 α' can be calculated at $P = 1, 2, \cdots, 6$MPa for temperatures from $300K$ to $574K$ at intervals of $10K$. α' at $303K = 5.8 \times 10^{-4} \pm 0.004$ at the equilibrium vapor pressure and $5.4 \times 10^{-4} \pm 0.004$ at 6MPa. The average α' from 25° to 70° is 5.8×10^{-4} as compared to 6.49×10^{-4} from Rabinovitch [54].

3.2.4 Isotope Effects

The molar volume isotope effect (MVIE) is obtained with good precision as follows. The PVT measurements on $(CH_2OH)_2$ and $(CH_2OD)_2$ were made at approximately the same temperatures and pressures. Therefore, for each molar volume measured for $(CH_2OD)_2$ at T and P $(V(T,P))$ the corresponding molar

volume for $(CH_2OH)_2$ ($V'(T', P')$) can be corrected for by using

$$V'(T,P) = V'(T',P') + \int_{T'}^{T} \alpha'(P')dT - \int_{P'}^{P} \kappa'(T')dP \qquad (3.18)$$

α' and κ' are interpolated from Eqn. 3.16 and Eqn. 3.13 respectively. MVIE is calculated as $\ln(V'/V)$ for each experimental temperature, and fit to the following equation

$$\text{MVIE} = \ln(V'/V) = D_0(T) + D_1(T)P \qquad (3.19)$$

The MVIE for $(CH_2OH)_2$ is pressure independent within the precision of our experiment (0.01%), therefore $D_1(T)$ is set to zero. The MVIE is given in terms of $D_0(T)$ for each temperature and they are listed in Table 3.8.

The MVIE as a function of T is plotted in Fig. 3.8. As in the case of H/D substitution in water and other hydrogen bonded liquids [36,54], the MVIE for $(CH_2OH)_2/(CH_2OD)_2$ is negative but small. MVIE (303) $= -0.0052 \pm 0.001$ from the present data. Rabinovitch reported [54] MVIE (293) and MVIE (343) as -0.0014 and -0.0016 respectively. From an independent measurement of the densities of $(CH_2OH)_2$ and $(CH_2OD)_2$ using a Mettlar Paar (DMA 60) vibrating tube densitometer, we obtain MVIE (303) $= -0.0056$. In view of the fact that these two results were obtained from two separate experiments using two different instruments, but on the same sample, the agreement is good. The MVIE curve shows the normal characterstic curvature observed for benzene, acetone, and methanol [36]. The abberant points at 350 and $398K$ are due to unknown causes.

Table 3.8: Parameters of Eqn. 10

#	T/K	$F(T)$	$10^9\sigma^2$
1	303.542	−0.0052	1
2	323.160	−0.0051	5
3	348.483	−0.019	1
4	372.657	−0.048	7
5	398.369	−0.049	34
6	423.891	−0.035	2
7	447.015	−0.064	30
8	498.109	−0.083	83
9	522.309	−0.053	13
10	548.42	−0.069	35
11	573.389	−0.096	97

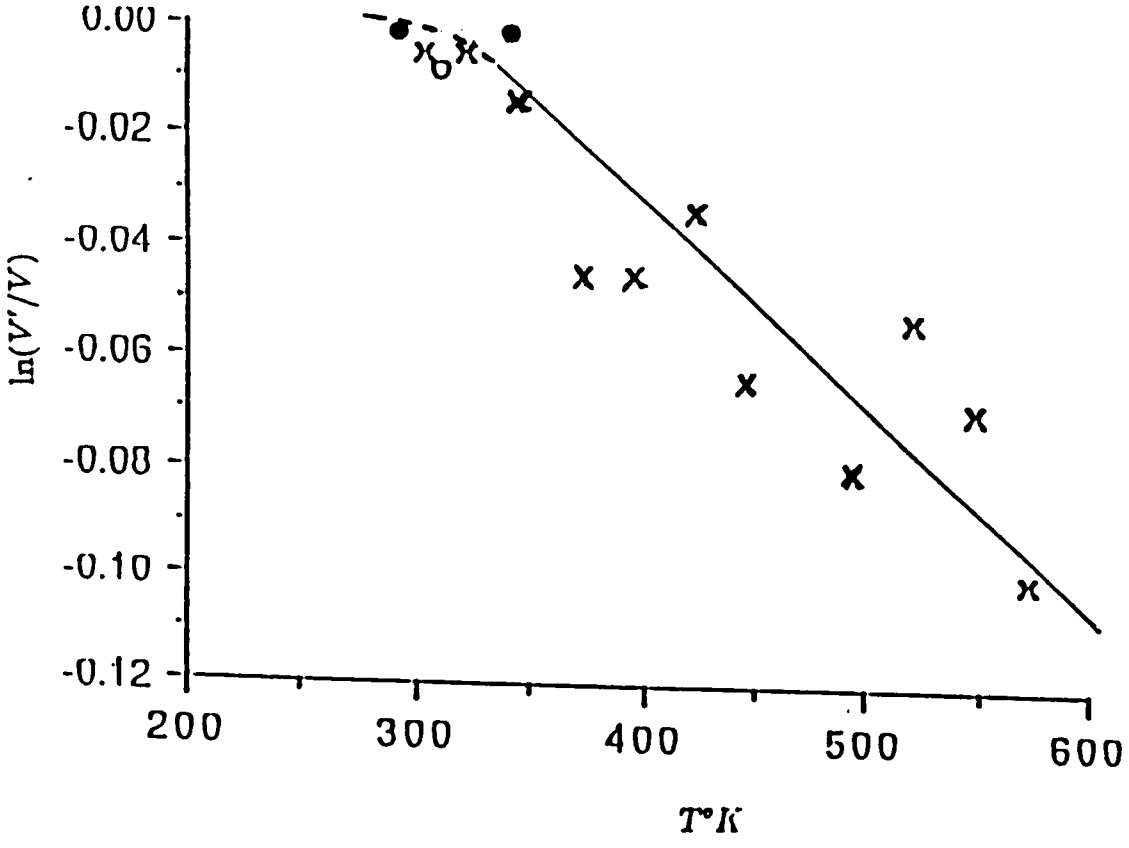


Figure 3.8: Plot of $\ln(V'/V)$ vs T; × This work PVT apparatus, • Ref [54], ○ This work DMA-60 Densitometer, – Calc. from Eqn. 3·10

If molar volume measurements are carried out at temperatures above $573K$ and extending up to the critical temperature $647K$, extreme curvature is expected in the high temperature region (Fig. 3.6). In that case Eqn. 3.12 would be inadequate to represent the experimental data and some high temperature corrections would become necessary. Kooner and Van Hook [36] have calculated such high temperature correction terms (HTCOR) for measurements of benzene, acetone amd methanol between a cutoff temperature T^* and the critical temperature T_c'. Such corrections if applied to Eqn. 3.12 would then yield,

$$\ln(V'(P)/\mathrm{m}^3/\mathrm{mol}) = \sum_{i=0}^{2} B_i T^i + \mathrm{HTCOR}$$

$$\mathrm{HTCOR} = 0 \ \mathrm{for} T < T^*$$

$$\mathrm{HTCOR} = B_3(T_c' - T)^{1/2} + B_4(T - T^*)^j \ \mathrm{for} T^* < T < T_c'.$$

Likewise, the temperature dependence of the orthobaric isothermal compressibility of the protio isomer would be represented by

$$\ln(\kappa^{o'}/\mathrm{MPa}^{-}1) = \sum_{i=0}^{2} C_i T^i + C_3/(1 - T/T_c')^{0.5}$$

instead of Eqn. 3.14, and the coefficient of thermal expansion would be

$$\alpha' = \sum_{i=1}^{2} i B_i T^{i-1} + d(\mathrm{HTCOR}')dT; \quad 303 < T < 647 \quad (3.20)$$

$$d(\mathrm{HTCOR}')dT = 0 \ \text{for} \ T < T^*$$

$$d(\mathrm{HTCOR}')dT = \frac{-B_3/2}{(T_c' - T)^{1/2}} + jB_4(T - T^*)^{j-1} : \ T^* < T < T_C'.$$

For the present range of temperature $303 < T/K < 574$ these corrections are not necessary.

Returning to the original discussion of MVIE's, the orthobaric MVIE's are obtained from

$$\ln\left(\frac{V^{0\prime}(P^{0\prime})}{V^{0}(P^{0})}\right) = \ln\left(\frac{V'(P^{0})}{V^{0}(P^{0})}\right) - \int_{P^0}^{P^{0\prime}} \kappa' dP \tag{3.21}$$

This integration is over a narrow pressure range. Since we are much below the critical temperature ($374°C$) the compressibility is assumed to be constant over the range of integration. So,

$$\kappa' dP = \kappa^{0\prime}(P^{0\prime} - P^{0}) = \kappa^{0\prime}(\ln(P^{0\prime}/P^{0})P^{0} \tag{3.22}$$

$\ln(P^{0\prime}/P^{0})$ is obtained from Eqn. 3.6 and P^{0} is obtained from Eqn. 3.6 and Eqn. 3.5. The orthobaric MVIE's are given in Table 3.9. The isobaric and orthobaric MVIE's are indistinguishable within the experimental error over the present range of measurements.

Isotope effects on the compressibilities can be recovered from Eqn. 3.13, Eqn. 3.14, and Eqn. 3.19.

$$\Delta\kappa = -(d\ln V'/dP) - (d\ln V/dP) = -D_1 T. \tag{3.23}$$

So at each experimental temperature

$$\frac{\Delta\kappa(T)}{\kappa'(T)} = D_1(T)/\sum_{i=1}^{2} iA_i(P - P^{0})^{i-1}. \tag{3.24}$$

The pressure dependence of the MVIE is very small and has been set to zero within the precision of the present experiment ($D_1 T$ in Eqn. 3.19). Therefore Eqn. 3.24 cannot be used for calculating the compressibility isotope effect. The

Table 3.9: Orthobaric MVIE's for ethylene glycol

#	T/K	MVIE $\ln(V^{0'}(P^{0'})/V^{0}(P^{0}))$
1	303.542	−0.00525
2	323.160	−0.00521
3	348.483	−0.02003
4	372.657	−0.04851
5	398.369	−0.04945
6	423.891	−0.03581
7	447.015	−0.06354
8	498.109	−0.08199
9	522.309	−0.05309
10	548.419	−0.06875
11	573.389	−0.09825

isothermal compressibility for the protio and deuterio isomers can be calculated at a common temperature using Eqn. 3.14 or Eqn. 3.15. From our data we calculate the isotope effect on isothermal compressibility $(\Delta\kappa/\kappa')_P$ at $303K$ as -0.01768 ± 0.002 ($\Delta\kappa = \kappa_H - \kappa_D$). The subscript P denotes that the liquids are being compared at identical pressures (zero pressure in this case). The magnitude of the isotope effect is comparable to that of methanol [36] -0.022 ± 0.002 at $303K$. We have been unable to find any other data in the literature on the isotopic differences of isothermal compressibility of ethylene glycol. However it is possible to compare our data with the adiabatic compressibility data of Rabinovitch [54] with the use of the thermodynamic relationship

$$\kappa_{iso} = \kappa_{ad} + \frac{\alpha T}{C_p^* \rho} \tag{3.25}$$

where α is the coefficient of thermal expansion, ρ is the density and C_p^* is the specific heat (*i.e.*, the heat capacity per mass) at constant pressure. From the Rabinovitch data for adiabatic compressibility, expansivity, density, and the heat capacity data [59] and Eqn. 3.25 the isotope effect is calculated to be $\Delta\kappa/\kappa = -0.0209 \pm 0.002$ at $303K$ and -0.019 ± 0.002 at $313K$ compared to the present value of $-0.0176(303K)$. The present experimental values also increase with temperature and become $+0.0017$ at $573K$. This is a sigificant increase in the magnitude of the compressibility IE. The sensitivity to temperature can be rationalised in terms of the external overall motions of the molecules and will be further discussed in the following chapter.

The expansivities for $(CH_2OH)_2$ were calculated from Eqn. 3.17 for a range of

temperatures at pressures from 1–6MPa. Isotope effects on isobaric expansivities can be recovered from Eqn. 3.16 and Eqn. 3.19.

$$\Delta\alpha = \frac{d\ln V'}{dT} - \frac{d\ln V}{dT} = \frac{dD_0(T)}{dT} + \frac{pdD_1(T)}{dT}$$

and at P^0 or $P = 1, 2, \cdots, 6\text{MPa}$

$$\frac{\Delta\alpha}{\alpha'} = \Delta\alpha/(\sum_{i=1}^{2} iB_i(P)T^{i-1})dT.$$

Least squares fit of the $D_0(T)$ parameters (Eqn. 3.19 and Table 3.8) with the intercept forced through the reported MVIE at $298K$ [54] $= -0.0014$ yields

$$\begin{aligned} D_0(T) &= -0.0745 + 3.305 \times 10^{-4}T - 1.09 \times 10^{-9}T^3 \\ \sigma^2 &= variance = 3.24 \times 10^{-5} \end{aligned}$$

The experimental IE on the expansivity $\Delta\alpha/\alpha$ is -0.0036 ± 0.0021 at $313K$. A reported [54] value in the temperature range 293 to $343K$ is -0.0046. The isotope effect becomes large at high temperature. The above experimental results and their correlation with theory are discussed in the next chapter.

3.3 Critical Solution Temperature (CST)

The coexistence curve for $(CH_2OH)_2 + CH_3NO_2$ was studied for the first time in 1973 [29] and the critical solution temperature at 1 atmosphere reported. The present data extends from 1 bar to 500 bars, at intervals of 50 bars. The CST data is given in Table 3.10. The measurements were made at 10–12 different

Table 3.10: Phase separation data for $(CH_2OH)_2 + CH_3NO_2$ system

#	p/bars	$X_{(CH_2OH)_2}$	$T°C$
1	1.8	0.1613	36.266
2	1.5	0.2251	38.355
3	1.0	0.2603	38.773
4	1.3	0.2857	39.339
5	1.6	0.3218	39.797
6	1.1	0.3445	39.825
7	1.2	0.3702	39.934
8	1.3	0.3932	39.948
9	1.4	0.4329	39.348
10	5.7	0.4808	38.841
11	1.4	0.4887	38.631
12	1.1	0.5106	37.479
13	1.2	0.5337	36.799
14	8.8	0.5629	35.259
15	25.1	0.1631	36.293
16	25.2	0.2251	38.386
17	25.1	0.2603	38.875
18	25.1	0.2857	39.236
19	25.0	0.3218	39.750
20	25.0	0.3445	39.838
21	25.0	0.3702	39.947
22	25.0	0.3932	39.848
23	25.1	0.4329	39.365
24	25.0	0.4808	38.807
25	25.1	0.4887	38.682
26	25.0	0.5106	38.541
27	25.0	0.5337	36.822
28	25.1	0.5629	35.272
29	50.1	0.1631	36.327
30	50.0	0.2251	38.464
31	50.1	0.2603	39.041
32	50.1	0.2857	39.276
33	50.0	0.3218	39.764
34	50.1	0.3445	39.868
35	50.0	0.3702	39.965
36	50.0	0.3932	39.979
37	50.0	0.4329	39.471
38	48.5	0.4808	38.916
39	50.3	0.4887	38.713
40	52.5	0.5106	37.813

Continuation of Table 3.10

#	p/bars	$X_{(CH_2OH)_2}$	$T°C$
41	50.0	0.5337	36.822
42	102.6	0.1631	36.404
43	100.0	0.2251	38.503
44	100.6	0.2603	39.130
45	100.3	0.2857	39.451
46	100.1	0.3218	39.885
47	100.1	0.3445	39.929
48	97.4	0.3702	40.061
49	100.3	0.3932	40.041
50	100.2	0.4329	39.508
51	100.1	0.4887	38.731
52	84.3	0.5106	37.630
53	100.6	0.5337	36.941
54	150.4	0.1631	36.457
55	150.0	0.2251	38.636
56	146.5	0.2603	39.289
57	150.0	0.2857	39.638
58	150.1	0.3218	39.953
59	150.2	0.3445	40.008
60	150.1	0.3702	40.131
61	150.0	0.3932	40.189
62	149.8	0.4329	39.535
63	132.7	0.4808	38.863
64	150.0	0.4887	38.756
65	150.2	0.5337	37.032
66	200.6	0.1631	36.514
67	199.6	0.2251	38.757
68	200.3	0.2603	39.303
69	202.2	0.2857	39.673
70	200.0	0.3218	40.025
71	200.1	0.3445	40.090
72	199.8	0.3702	40.230
73	200.0	0.3932	40.118
74	200.1	0.4329	39.598
75	203.6	0.4808	38.94
76	200.2	0.4887	38.752
77	200.2	0.5337	37.292
78	250.6	0.2251	38.847
79	250.1	0.2603	39.401
80	250.2	0.2857	39.704

Continuation of Table 3.10

#	p/bars	$X_{(CH_2OH)_2}$	$T°C$
81	250.1	0.3218	40.112
82	250.4	0.3445	40.163
83	250.1	0.3702	40.298
84	250.2	0.3932	40.193
85	248.9	0.4329	40.009
86	242.5	0.4808	38.883
87	250.0	0.4887	38.802
88	250.2	0.5629	37.456
89	300.0	0.1631	36.682
90	299.8	0.2251	38.964
91	301.1	0.2603	39.401
92	300.0	0.2857	39.837
93	300.0	0.3218	40.183
94	300.0	0.3445	40.225
95	299.7	0.3702	40.324
96	300.1	0.3932	40.300
97	300.1	0.4329	39.922
98	300.0	0.4808	39.072
99	300.0	0.4887	38.847
100	351.4	0.1631	36.754
101	350.2	0.2603	39.801
102	350.0	0.2857	39.900
103	350.4	0.3218	40.281
104	350.0	0.3445	40.310
105	350.1	0.3702	40.482
106	350.3	0.3932	40.398
107	348.2	0.4329	39.955
108	350.0	0.4887	38.898
109	349.3	0.5337	37.093
110	400.1	0.1631	36.828
111	400.3	0.2251	39.155
112	400.0	0.2603	39.931
113	400.0	0.3218	40.371
114	399.0	0.3445	40.356
115	400.0	0.3702	40.558
116	400.1	0.3932	40.507
117	400.1	0.4329	40.183
118	399.8	0.4887	38.869
119	450.4	0.1631	36.903
120	450.0	0.2251	39.281

Continuation of Table 3.10

#	p/bars	$X_{(CH_2OH)_2}$	$T°C$
121	450.1	0.2603	39.997
122	449.3	0.2857	40.013
123	450.2	0.3445	40.437
124	450.2	0.3702	40.669
125	450.1	0.3932	40.552
126	450.6	0.4329	40.276
127	450.0	0.4887	38.982
128	500.0	0.2251	39.365
129	500.6	0.2603	40.044
130	500.4	0.2857	40.096
131	500.0	0.3445	40.499
132	500.0	0.3702	40.745
133	499.6	0.3932	40.632
134	497.1	0.4329	40.549
135	500.0	0.4887	39.061

concentrations. Figure 3.9 is a plot of the data at 1 bar. The data at 1 bar were fitted to the scaling equation of the coexistence curve,

$$|(X - X_c)| = A(1 - T/T_c)^{\beta} \tag{3.26}$$

In Fig. 3.9 the curves seem to appear slightly skewed. In an attempt to account for the skewing a fit was carried out with the expression

$$|(X - X_c)| = A(1 - T/T_c)^{\beta} + B(1 - T/T_c) \tag{3.27}$$

These results are reported in Table 3.11. However since there was no improvement in the variance of the the fit the additional term was dropped. It appears the diameter is perpendicular within the experimental precision. Thus the fits were carried out by using Eqn. 3.26 and the following functional forms of Eqn. 3.26 in order to determine the pressure dependences of the critical parameters T_c, X_c, β and A (Eqns. 3.28–3.32).

$$|X - X_c| = A(1 - T/T_c)^{\beta} \tag{3.28}$$

$$|X - X_c| = A\left(1 - \frac{T}{T_c^0 + cp}\right)^{\beta} \tag{3.29}$$

$$|X - X_c - B_p| = A\left(1 - \frac{T}{T_c^0 + cp}\right)^{\beta} \tag{3.30}$$

$$|X - X_c| = (A + B_p)\left(1 - \frac{T}{T_c^0 + cp}\right)^{\beta} \tag{3.31}$$

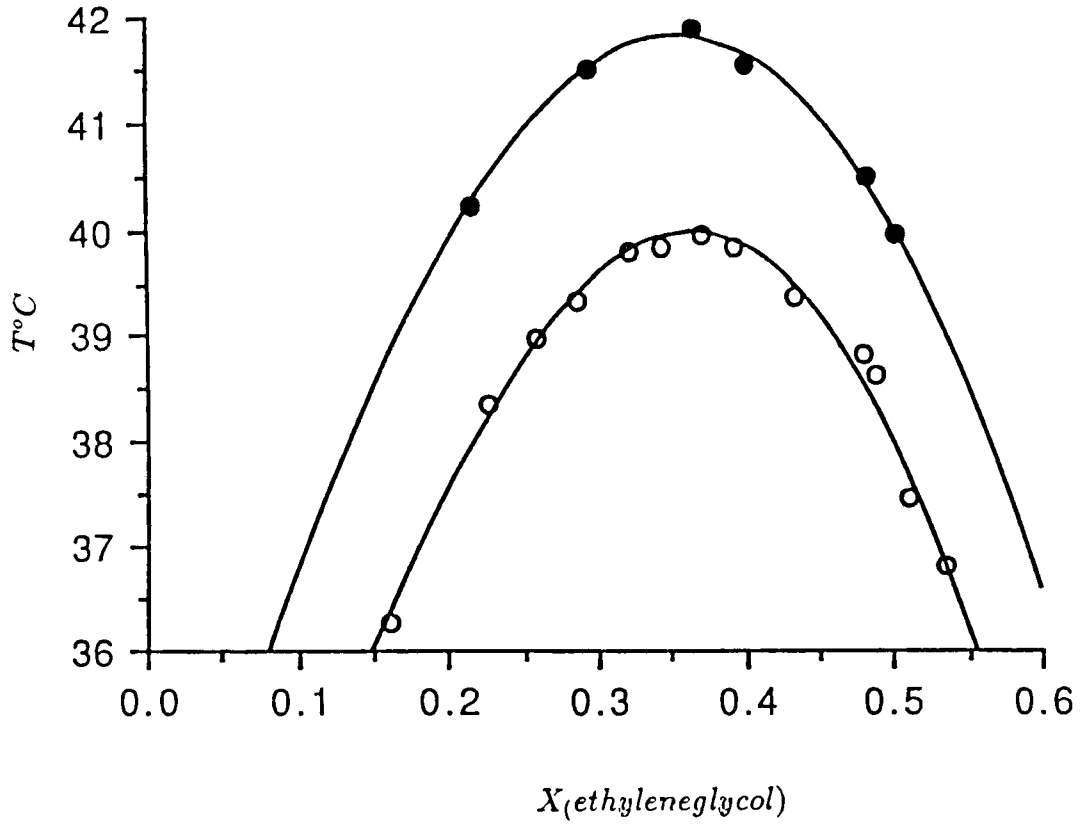


Figure 3.9: CST curves at 1 atmosphere, • : $(CH_2OD)_2 + CH_3NO_2$, ∘ : $(CH_2OH)_2 + CH_3NO_2$

Table 3.11: Least Squares Fit of Phase Separation Data for $(CH_2OH)_2$+CH_3NO_2 System

Parameter	X_c	A	β	T_c/K	$c/K/bar \times 10^{-5}$	$B/bar^2 \times 10^7$	Variance $\times 10^4$
Eqn. 3.28 Atm data	0.361 ± 0.0035	2.103 ± 0.033	0.537 ± 0.06	313.135 ± 0.045			1.23
Eqn. 3.28 all data	0.355 ± 0.002	1.905 ± 0.03	0.507 ± 0.028	313.145 ± 0.02			1.4
Eqn. 3.29 all data	0.363 ± 0.0011	1.84 ± 0.11	0.503 ± 0.012	313.053 ± 0.006	0.0016 ± 4.3		1.62
Eqn. 3.30	0.363 ± 0.0018	1.84 ± 0.14	0.504 ± 0.015	313.058 ± 0.01	0.0016 ± 2.3	-17.4 ± 65.0	1.62
Eqn. 3.31	0.363 ± 0.011	1.85 ± 0.14	0.505 ± 0.015	313.06 ± 0.011	0.0016 ± 2.3	338 ± 140	1.58
Eqn. 3.32	0.363 ± 0.0011	1.87 ± 0.13	0.507 ± 0.013	313.061 ± 0.014	0.0015 ± 11.6	11.8 ± 2.2	1.41
Eqn. 3.27	0.359 ± 0.0018	1.61 ± 0.12	0.47 ± 0.014	312.974 ± 0.005	0.0015 ± 3.0	-0.341 ± 0.314	1.8
Eqn. 3.34	0.366 ± 0.0014	1.90 ± 0.12	0.51 ± 0.012	313.057 ± 0.0024	0.0016 ± 1.4	-1.58 ± 0.284	1.3
$t < 0.003$	0.367 ± 0.0012	2.377 ± 0.12	0.56 ± 0.04	313.1 ± 0.014	0.0015 ± 4.1		2.1

$$|X - X_c| = A\left(1 - \frac{T}{T_c^0 + cp + bp^2}\right)^{\beta} \tag{3.32}$$

The values of the parameters along with their standard deviation and the variances of the fits are also reported in Table 3.11. As can be seen from that Table, there is no pressure dependence for β, X_c and A for the $(CH_2OH)_2 + CH_3NO_2$ system. There is however a first order pressure dependence for T_c.

The actual equation used in the non–linear least square fitting of our data was of the form,

$$X = X_c + aA|(1 - T/T_c)|^{\beta} \tag{3.33}$$

where $a = +1$ if $X > X_c$ and -1 if $X > X_c$. The absolute value of the $1 - T/T_c$ term was used in order to avoid program termination if T for any data point became greater than the value of the parameter T_c during the fitting procedure.

Since β is defined only in the asymptotic limit near T_c, the proper description of a coexistence curve beyond the asymptotic range should include terms of higher order than the simple scaling term of Eqn. 3.26. Hence it is usual [60] to fit phase equilibrium data to extended expressions like

$$|(X - X_c)| = A(t)^{\beta}(1 + A't^{(\beta+0.5)} + \cdots) \tag{3.34}$$

where the second and higher terms constitute corrections. This expression represents the extended scaling hypothesis, and the term $(\beta + 0.5)$ is known as the Wegner correction [61]. Such corrections have been found useful for isobutyric acid + water [7] and $CS_2 + CH_3NO_2$ [11] but not useful for cyclohexane +

methanol [9] binary systems. The variance of the fit of our data to this equation is no smaller than the ones which did not include the Wegner correction and the additional terms are not considered any further. β remains close to 0.5 from this fit.

Phase separation data for the system $(CH_2OD)_2 + CH_3NO_2$ is given in Table 3.12. The data at one atmosphere is plotted in Fig. 3.9. That data and the complete data at all pressures was fit to Eqns. 3.26 and 3.29 respectively. The results of these fits are given in Table 3.13. A comparison of Tables 3.11 and 3.13 indicates that there is no effect of isotopic substitution on β, X_c and $c = dT_c/dP$.

We have measured the parameters describing the coexistence surface. The parameters X_c, A, and β are independent of pressure. The slope of the critical line dT_c/dP was found to be 0.0016 k/bar $\pm 4.3 \times 10^{-5}$. There is no effect of isotopic substitution on X_c, β, and dT_c/dP. $T_c(H) - T_c(D) = -2.01K$. The direction of the isotope effect on T_c is as expected. There is an isotope effect on the critical amplitude A, but it is not very well defined. The value for the critical exponent β is 0.5 which is not in agreement with the non–classical expectations for the limiting value, but is in agreement with classical mean field theory calculations. The implications of these observations will be discussed in the next chapter.

Table 3.12: Phase separation data for $(CH_2OD)_2 + CH_3NO_2$ System

#	P/*bars*	X	T°C
1	1.1	0.2156	40.234
2	1.2	0.2959	41.481
3	1.2	0.6459	41.881
4	5.7	0.4008	41.553
5	1.1	0.4819	40.501
6	1.4	0.5019	39.959
7	26.9	0.2156	40.274
8	17	0.2959	41.499
9	25.1	0.3646	41.921
10	25.2	0.4819	40.544
11	25.1	0.5019	39.998
12	50.3	0.2959	41.554
13	50.7	0.3646	41.96
14	58.1	0.4008	41.426
15	100.7	0.2156	40.398
16	101.0	0.2959	41.61
17	99.3	0.3646	42.011
18	109.8	0.4008	41.475
19	98.8	0.4819	40.598
20	101.1	0.5019	40.062
21	147.4	0.2156	40.484
22	150.3	0.2959	40.57
23	147.4	0.5019	40.15
24	200.2	0.2959	41.736
25	200.3	0.4008	41.58
26	200.1	0.4819	40.683
27	200.1	0.5019	40.16
28	303.1	0.2156	40.717
29	300.5	0.2959	41.866
30	300.4	0.4008	41.744
31	313.2	0.4819	40.838
32	299.8	0.5019	40.284
33	350.6	0.2156	40.795
34	400.0	0.2959	41.993
35	401.1	0.3461	42.184
36	403.3	0.4008	42.053
37	409.3	0.4819	40.924
38	400.5	0.5019	40.389
39	450.3	0.2156	40.957
40	448.6	0.5019	40.433

Continuation of Table 3.12

#	P/*bars*	X	T°C
41	500.1	0.2959	42.133
42	500.3	0.3461	42.255
43	501.6	0.4008	42.185
44	500.5	0.4819	41.074
45	500.8	0.5019	40.51

Table 3.13: Least Squares Fit of Phase Separation Data for $(CH_2OD)_2$+CH_3NO_2 System

Parameter	X_c	A	β	T_c/K	$c/K/bar$	Variance
Equation 3.28 Atm data only	0.371 ± 0.014	1.46 ± 0.25	0.505 ± 0.06	315.035 ± 0.058		8.28×10^{-4}
Equation 3.29 all data	0.36 ± 0.0029	1.77 ± 0.051	0.506 ± 0.015	315.04 ± 0.012	$0.0016 \pm 2.1 \times 10^{-4}$	1.18×10^{-4}

CHAPTER 4

Discussion

In section 4.1 we discuss the PVT properties of $(CH_2OH)_2$ and their isotope effects and make an attempt to discuss the experimental results according to the condensed phase isotope effect theory. Section 4.2 deals with the pressure dependence and isotope effects on the coexistence curve parameters for the ethylene glycol–nitromethane binary system.

4.1 VPIE and MVIE

We have measured the vapor pressure of $(CH_2OH)_2$ and $(CH_2OD)_2$ from $373K$ up to $573K$. A literature survey indicates that most prior data for the protio isomer ended around $500K$. Decomposition has been reported [52] at $340K$ (from the evidence of increasing pressure with time in a static measurement). There was no such evidence within the present ranges of temperature; and the fits of all the data points to Eqn. 3.1 are not noticeably worse than has been reported by previous authors. There is no prior information on the vapor pressures of $(CH_2OD)_2$.

The VPIE remains normal ($P_H > P_D$) over the entire temperature range (Table 3.5 on page 39 and Fig. 3.4 on page 40). A theoretical approach to the

VPIE has been made by Bigeleisen [37] and numerous quantitative applications of his approach may be found in the literature [31]. The VPIE of ethylene glycol is well represented by the AB Eqn. 1.13. In this Eqn. A represents contributions from lattice motions and internal motions which include internal rotation and certain skeletal motions (but the skeletal modes do not show marked isotope dependence [62]). B represents the contribution of the zero point energy changes of the higher ($\nu > 2\pi$) internal frequencies. The constant C serves as a sink for higher order correction terms and other real difficulties such as temperature dependent force constants (due to lattice expansion on warming), anharmonicities, etc. The fit of the present results to Eqn. 1.13 is satisfactory. A/T^2 is positive and greater in magnitude than B/T as is expected for a normal VPIE. In the usual case C only makes a small contribution. To that extent our measurements are in reasonable accord with the theory. A more detailed test of the correspondence between theory and experiment is possible using the Stern–Van Hook–Wolfsberg [39]model which has been successfully applied to the benzene–cyclohexane systems [63].

The recommended procedure [39] involves calculation of sets of spectroscopic frequencies and frequency shift data using an isotope independent force field, consistent with the observed frequencies. For $(CH_2OH)_2$ we do not have a detailed FG calculation of spectroscopic properties, but in their absence we have tested the consistency in the thermodynamic measurements and spectroscopic calculations in the following manner. At low enough temperatures gas imperfec-

tions and terms involving the molar volume of liquid may be reasoned to make negligible contributions to the vapor pressure ratio. We can then calculate the contributions of both the external and the internal frequencies (Eqn. 1.13) in terms of the isotopic differences in the frequency shifts on condensation [62,64,65] expressed as a ratio of the reduced partition functions for the vapor and condensed phases. In the absence of detailed information of force constants we have obtained consistency by requiring that the ratios of the observed frequency shifts on condensation for the deutero isomer be the same as that for the protio isomer. We have considered only those frequencies which are isotope sensitive, namely the 2 OH and OD stretching frequencies and the OH and OD bonded librational frequencies lying at 1400 and $700cm^{-1}$ and 974 and $450cm^{-1}$ respectively. The neccessary spectroscopic data is given in Table 4.1. There is considerable scatter

Table 4.1: Assignment of the vibrational spectrum of ethylene glycol

	$(CH_2OH)_2$		$(CH_2OD)_2$
Assignment	liquid	liquid/solution	liquid
νOH	3275	0.897 ± 0.002^a	2475
τOH	1405	1.068 ± 0.002^a	974 (985)
τOH	700 (650)	1.898 ± 0.015^b	450 (465)

[a] equal to $\pm 4cm^{-1}$ in frequency shift

[b] equal to $\pm 30cm^{-1}$ in frequency shift

in the reported frequencies (Table 4.1).

$$\frac{\ln P'}{P} = \ln\left[\prod_i^4 \frac{f(u_i^{\mathrm{H}})_{liq}}{f(u_i^{\mathrm{H}})_{soln}} / \frac{f(u_i^{\mathrm{D}})_{liq}}{f(u_i^{\mathrm{D}})_{soln}}\right]$$

where

$$f(u_i) = \frac{\exp(-u_i/2)}{1-\exp(-u_i)}$$

The theoretical VPIE thus obtained is $\ln P'/P = 0.177 \pm 0.04$ at $300K$. The experimental isotope effect $\ln P'/P$ at $300K$ is calculated from Eqn. 3.6 as 0.1506 ± 0.0004 at $300K$. While the model is highly approximate, it gives an idea about the physical meaning of the isotope effect. All OH and OD bands are very broad due to hydrogen bridge bonding within the liquid. It is clear that the best physical understanding will be achieved by an interactive approach using both spectroscopic and thermodynamic information.

Isotope effects on liquid compressibilities have been rationalised [33] by using a partition function assumed to factor into hard sphere (HS), attractive, internal vibrations and librational parts,

$$Q = Q_{HS}Q_{att}Q_{vit}Q_{lit}$$

$$1/(\kappa VRT) = -(\partial^2 \ln Q)/\partial V^2$$

where the important contributions are from hard sphere, librational and intermolecular (attractive) terms. The hard–sphere contribution has been evaluated by Stillinger as [66]

$$1/\kappa_{\mathrm{HS}} = \frac{RT}{V}\left[\frac{1+2y}{(1-y)^2}\right]^2 \qquad (4.1)$$

where $y = \pi\rho d^3/6$ is the volume fraction of hard sphere molecules, ρ is the number density (N/V; *i.e.*, the reciprocal of the volume per molecule), and d is the hard sphere diameter. y can also be determined from experimental data with the following Eqn. [67].

$$RT\left(\frac{1+y+y^2}{(1-y)^3}\right) = n(\Delta H_{vap} - RT) \tag{4.2}$$

ΔH_{vap} is calculated from the vapor pressure data given in Table 3.1 on page 31. Eqn. 4.2 yields $y = 0.5574$ using $n = 1$. An independent calculation of y from the density of the liquid yields $y = 0.599$, in line with that determined by Eqn. 4.2. Substituting $y = 0.5574$ in Eqn. 4.1 results in the estimate $1/\kappa_{HS} = 117.0RT/V$. The internal–vibration and librational terms can be approximated in terms of a harmonic oscillator model

$$\ln(Q_{vit}Q_{lit}) = \sum_{i=1}^{(3n-3)N} \ln\left[\frac{\exp(-u_i/2)}{1-\exp(-u_i)}\right]. \tag{4.3}$$

In Eqn. 4.3 n is the number of atoms per molecule and N the Avogadro number. $u_i = h\nu_i/kT = hc\omega_i/kT$ where the normal mode vibrational frequencies ν_i or ω_i have units of s^{-1} or cm^{-1} respectively. Combination of Eqns. 4.1 and 4.3 gives

$$\kappa_R^{-1}(vib.lib) = \frac{V}{RT\kappa_{vit.lit}} = \sum_i \left(\gamma_i^2 S(u_i) + \gamma_i\left(1 - \frac{\partial \ln \gamma_i}{\partial \ln V}\right)T(u_i)\right) \tag{4.4}$$

$$T(u_i) = \frac{u_i}{2}\frac{1+e^{-u_i}}{1-e^{-u_i}} \tag{4.5}$$

$$S(u_i) = T(u_i) - u_i^2 e^{-u_i}/(1-e^{-u_i})^2. \tag{4.6}$$

For high u_i, $\lim(T(u_i)) = \lim(S(u_i)) = u_i/2$ and at small u_i, $\lim(S(u_i)) = u_i^2/6 \approx 0$ and $\lim(T(u_i)) = 1 + S(u_i)/2 \approx 1$. In Eqn. 4.4 γ_i are the Gruneisen

coefficients of the individual frequencies, $\gamma_i = -(d\ln u_i/d\ln V)$. The internal and the librational contributions can be evaluated independently if the pressure (volume) dependence of the various frequencies are known. In the absence of such information for ethylene glycol we have used the pressure dependence of the O–H frequencies observed for water. For the O–H streches $d\nu_i/dP = -3.77cm^{-1}/kbar$ [68], equivalent to a Gruneisen coefficient, $\gamma_i \simeq 1.2 \times 10^{-3}$. For the upper limit case Eqn. 4.4 leads to the estimate $1/\kappa_{vit} = 1.97RT/V$, assuming $\partial \ln \gamma_i/\partial V << 1$ and $\gamma_i^2 << \gamma_i$. The intermolecular libration region $\approx$ 300–$1000cm^{-1}$ for water shows no significant pressure variance upto $11.3kbar$ [68] *i.e.*, $(d\nu_i/dP)_{lit} = 0$, $\gamma_{i,lit} = 0$. This implies that there is no librational contribution to the compressibility. This conclusion is somewhat suspect.

The contribution of the attractive part of the potential is obtained following the treatment used by Arakawa and Kojima [67]. $Q_{att} = \exp(-\phi/kT)$ where ϕ is taken as proportional to the $-j$th power of the volume; j being a parameter. Making use of the partition function for a hard sphere fluid they derive ϕ to be the negative energy of vaporization

$$\phi = -\Delta H_{vap} - RT = \text{constant}/V^j. \tag{4.7}$$

$j = 0.33$ is calculated from the experimental V and ΔH_{vap}, so $1/\kappa_{att} = 9.46RT/V$. Then collecting terms from Eqns. 4.3 and 4.4 the complete equation for the compressibility is

$$\frac{1}{\kappa} = \frac{RT}{V}\left[\left(\frac{1+2y}{(1-y)^2}\right)^2 + 3\gamma_{lit} - j(j+1)\left(\frac{H_{vap}-H_{liq}}{RT} - 1\right)\right] \tag{4.8}$$

From the relative contributions of Eqn. 4.8 clearly the hard sphere contribution is most important. κ calculated from Eqn. 4.8 is $2.1 \times 10^{-4}\text{MPa}^{-1}$. Even though the calculated value is lower than the observed ($3.73 \times 10^{-4}\text{MPa}^{-1}$) we can conclude that the above approach models the liquid compressibility well enough to interpret the physical causes of the compressibility and the isotope effect.

The isotope effect on the isochoric compressibility has contributions from the hard sphere, vibrational, and attractive terms. It can be rationalized by expressing Eqn. 4.8 in the form

$$\frac{\Delta(1/\kappa)}{(1/\kappa)} = \frac{\Delta\kappa_{\text{HS}} + \Delta\kappa_{vit} - \Delta\kappa_{att}}{1/\kappa} \tag{4.9}$$

Any isotope effect on $1/\kappa_{vit}$ results only from an isotope dependent Gruneisen $\gamma_{vit} = (\gamma_D/\gamma_H)$. For water $\gamma_H = 1.2 \times 10^{-3}$ and $(\gamma_D/\gamma_H) = 0.725$. However the vibrational contribution is very small and can be neglected in comparison with the other terms. The attractive contribution is obtained from the isotope effect on ΔH_{vap}. The vapor pressure data yields $(\Delta H_{vap,D} - \Delta H_{vap,H})/\Delta H_{vap,D} = 3.11 \times 10^{-3}$, which also is small. Therefore under conditions of equal volume the hard sphere isotope effect is dominant. This contribution can be calculated from the isotope effects on the mean square amplitudes [69] of O–H and O–D or from differentiating Eqn. 4.7 with respect to isotope. The later method gives $\Delta y/y = -0.0007$. The calculated isotope effect from Eqn. 4.9 is -0.035 ± 0.0003 compared to the experimental -0.0176 ± 0.002. The error bar in the calculated IE is obtained from the assumption that $\delta\Delta y/y = \pm 0.0002$. This is a crude approximation and it is difficult to justify our use of the hard sphere model for

ethylene glycol. However, we are more interested in the isotope effect rather than the physical property itself and in the absence of any other reasonable approximation we have forcibly done so. It is therefore almost exclusively rationalized in terms of the external overall motions of the molecule in the intermolecular force field.

The expansivity isotope effect is large and negative and is associated primarily with the high frequency isotope sensitive vibrations. A rationale has been outlined [33] using the partition function model shown above and applying

$$\alpha = \kappa(dP/dT)_V = \kappa(d^2 ln(Q)/dVdT) \tag{4.10}$$

so,

$$\Delta\alpha = (dP/dT)\Delta\kappa + \kappa\Delta(dP/dT). \tag{4.11}$$

κ becomes large at high temperatures. The volume and α also increase markedly. Thus $(dP/dT)_v = \alpha/\kappa$ must be small at high temperature and the second term in Eqn. 4.11 becomes dominant as the temperature increases towards T_c. Therefore

$$\Delta\alpha = \kappa\Delta(dP/dT)_v = (d^2 \ln Q_{ext}/dVdT) + (d^2 \ln Q_{osc}/dVdT) \tag{4.12}$$

where the vibrational and librational parts of the partition function are described in terms of an oscillator model. The first term is small compared to the second and the effect reduces to a sum over oscillator partition functions.

$$\Delta\alpha = \kappa(RT/V)\sum_i (f(u_i') - f(u_i))(d\gamma_i/dT) \tag{4.13}$$

$u_i = h\nu_i/kT$, ν_i being the harmonic or anharmonic frequency and $f(u_i) = u_i/2 + u_i \exp(-u_i)/(1 - \exp(-u_i))$. $\gamma_i = -d\ln\nu_i/d\ln V$ is the Gruneisen coefficient for that particular frequency. For large u_i, $f(u_i) \rightarrow u_i/2$ and the isotope effect $\Delta f(u_i) = \Delta u_i/2$. $f(u_i) \rightarrow 1$ for small u_i and the isotope effect disappears. Thus only the high frequency vibrations, which also show a significant isotope dependence, are important. Once again we can use the temperature coefficient of the Gruneisen constants of the O–H and O–D stretching frequencies of water. γ_i is negative as shown before and has a small negative temperature coefficient $d\gamma_i/dT = -3.54 \times 10^{-5}$. The calculated $\Delta\alpha = -2.3 \times 10^{-6}$ leading to $\Delta\alpha/\alpha = -0.0031$, as compared to the experimental -0.0036 ± 0.0021. The agreement is fortuitous.It does however imply that our approximation for the frequencies and their pressure and temperature coefficients are reasonable.

As mentioned in the introduction, the treatment of condensed phase isotope effect [37] relates the theoretically available reduced partition function ratio RPFR = $\ln(f_c/f_v)$ to the measured vapor pressure isotope effect, VPIE = $\ln(P'/P)$ (plus volumetric correction terms).

$$\begin{aligned} \text{RPFR} &= \ln(P^{0'}/P^0) - (P^{0'}V^{0'} - P^0V^0)/(RT) + (1/RT) \\ &\quad \left[\int_0^{P^{0'}} \alpha'_v dP - \int_0^{P^0} \alpha_v dP\right] + \int_{V^0}^{V^*} (d\ln Q/dV)dV \end{aligned} \qquad (4.14)$$

where $V^{0'}$ and V^0 are condensed–phase molar volumes. The second term is the PV difference between the Gibbs and Helmholtz free energies while the third term expresses the non ideality correction in the vapor phase, $\alpha_v = (V_v - RT/P)$ and $\alpha'_v = (V'_v - RT/P')$, and V_v and V'_v are vapor–phase molar volumes. The

last term on the right hand side is the free energy change that results when one isotope is compressed or expanded from its equilibrium P^0V^0 state to a new condition P^*V^*, where it is in a congruent state with the other isotope. Singh and Van Hook [9] have discussed this term which results from the fact that the reduced distribution functions used to calculate RPFR are sensitive functions of molar volume. The RPFR is normally calculated for the case of equivalent distribution functions (the so–called congruent state) and in order to compare the calculation with experiment, a comparison should be made where the PES's are the same. It is usually assumed that when the isotopes being compared are in their orthobaric states, and at a common temperature, they are congruent and the last term is set to zero.

This hypothesis was verified experimentally by measuring the relevant isotope effects at high pressures and temperatures for acetone, benzene and methanol [36]. For all these compounds it was observed that the sum of the three terms in Eqn. 4.14 tends to zero at T_c. In other words SUM = RPFR $- \int_{V^0}^{V^*}(d\ln Q/dV)dV$ tends to zero as T_c is approached. Also from the thermodynamic identity of the condensed and vapor phase under critical conditions we can conclude that RPFR is close to zero or zero across the critical region [36]. Therefore $\int_{V^0}^{V^*}(d\ln Q/dV)dV = 0$. This leads to the conclusion that $V^* = V^o$, and that those samples of separated isotopes were in the congruent state when each was at its equilibrium molar volume and under its equilibrium vapor pressure.

We have evaluated the first two terms of Eqn. 4.14 from the present data as far as $T/T_c' = 0.88$. The results are presented in Table 4.2. We do not have

Table 4.2: Various terms in Eqn. 4.13

#	T	$\ln(P^{0'}/P^0)$ $(a) \pm 5.0 \times 10^{-4}$	$1/RT(P^{0'}V^{0'} - P^0V^0)$ $(b) \pm 0.0012$	$(a+b) \pm 0.0012$
1	303.542	0.1041	3.169×10^{-6}	0.1041
2	323.160	0.0817	4.093×10^{-6}	0.0818
3	348.483	0.0605	1.311×10^{-5}	0.0605
4	372.657	0.0459	3.13×10^{-5}	0.0459
5	398.369	0.0349	7.36×10^{-5}	0.0349
6	423.891	0.0272	2.41×10^{-4}	0.0275
7	447.015	0.0224	2.31×10^{-4}	0.0227
8	498.109	0.0167	-1.279×10^{-3}	0.0154
9	522.309	0.0155	-8.1×10^{-4}	0.0164
10	548.419	0.0152	-2.94×10^{-3}	0.0122
11	573.389	0.0153	-1.65×10^{-2}	-0.0011

the experimental information to calculate the vapor phase non ideality (third term) in the high temperature–high pressure region. For water, methanol, acetone, benzene [36] and methane [44] it is observed that as T_c is approached, the molar volume and the vapor non–ideality corrections each increase and become approximately equal at T_c. From the table it can be seen that the molar volume correction $((P'V' - PV)/RT)$ also increases towards $574K$. We expect the non–ideality corrections for ethylene glycol to exhibit similar behaviour. It thus becomes possible to estimate roughly the magnitude of the vapor nonideality corrections. Rearrangement of Eqn. 4.14 gives

$$\ln(P^{0'}/P^0) = \text{RPFR} + (P^{0'}V^{0'} - P^0V^0)/(RT) - (1/RT)$$

$$\left[\int_0^{P^{0'}} \alpha_v' dP - \int_0^{P^0} \alpha_v dP\right] - \int_{V^0}^{V^*} (d\ln Q/dV)dV. \quad (4.15)$$

The vapor nonideality correction is approximated at T_c' from the VPIE and the molar volume correction term, by setting the last term and RPFR to zero at the critical point. We obtain -0.0749 as the vapor nonideality correction which is comparable to the molar volume correction -0.0769 at T_c'. Experimental measurements of the vapor non–ideality are possible by measuring the n(inj),P curve before condensation. This data is useful only when the sample temperature is high and n (vapor) is large (see Chap. 2, Sec. 2.2). For compounds having relatively low vapor pressure like ethylene glycol, the precision of such measurements is expected to be poor. The above calculations could perhaps be used to determine the virial coefficients of the sample.

At high temperatures where loss of H–bonding occurs virial coefficients may be approximated assuming the Lennard–Jones potential for liquids [70].

$$B(T) = b_0 B^*(T^*) \quad (4.16)$$

where $T^* = kT/\epsilon$, $b_0 = 2/3\pi N\sigma^3$, and $\epsilon/k = 0.77T_c$. B^* is obtained for the corresponding T^* from Hirschfelder, Curtiss, and Bird [70]. σ is calculated from y (the hard sphere volume fraction) as $4.72A^o$ and Eqn. 4.16 yields $B'(T_c) = -252.5cc/mole$. $(B'/B)_{T_c}$ is then easily obtained by substituting B' and P' and P in the vapor nonideality correction term at the critical temperature. $(B'/B)_{T_c} = 0.9986$ indicating a very small virial coefficient isotope effect (VCIE). This observation is in agreement with the literature data on VCIEs of water and

methanol.

The physical interpretation may be seen from a plot of the orthobaric projection of $\ln V$ vs T shown in Fig. 4.1. The solid lines indicate orthobaric volumes of $(CH_2OH)_2$ and the dotted lines indicate $(CH_2OD)_2$ orthobaric volumes which are drawn at a different scale to avoid overlapping with the solid line. The low temperature end on the lower left hand side of the diagram shows the isotope effect on condensed–phase volume, $\ln(V^{0\prime}/V^0) = -0.0051$. Both the lower and the upper branches show the dotted line above the solid line because the low temperature MVIE is inverse and the low temperature VPIE is normal. The upper right part of the diagram indicates the isotopic ratio of vapor volumes at low pressure which can be calculated when the vapor pressure and the virial coefficient isotope effects, and the $P'V'_v$ product of the protio reference $P'V'_v = RT + B^{*\prime}P^{0\prime} + C^{*\prime}P^{0\prime 2}$ are known:

$$\begin{aligned}(V/V')_v &= (P^{0\prime}/P^0)\left[1 - \left[B^{*\prime}P^{0\prime}(\Delta B^{*\prime}/B^{*\prime} + \Delta P^0/P^{0\prime}) + C^{*\prime}P^{0\prime 2}\right.\right. \\ &\qquad \left.\left.(\Delta C^*/C^{*\prime} + 2\Delta P^0/P^{0\prime})\right] / \left[RT + B^{*\prime}P^{0\prime} + C^{*\prime}P^{0\prime 2}\right]\right]. \quad (4.17)\end{aligned}$$

At low enough temperatures both vapor phases exhibit ideal gas behaviour and the isotopic ratio of vapor volumes is approximately equal to the the inverse of the VPIE, $\ln(V_v^{0\prime}/V_v^0) = -\ln(P^{0\prime}/P^0$. With the rise in temperature the vapor pressure of $(CH_2OH)_2$ and $(CH_2OD)_2$ get closer (Table 3.5 on page 39). It is postulated [54] that $\ln(P'/P)$ crosses and above a certain temperature above a certain temperature P^0 will be $> P^{0\prime}$. The cross over has been established experimentally for methanol [36] as 443 K. For water $P^0(D_2O) < P^0(H_2O)$ upto

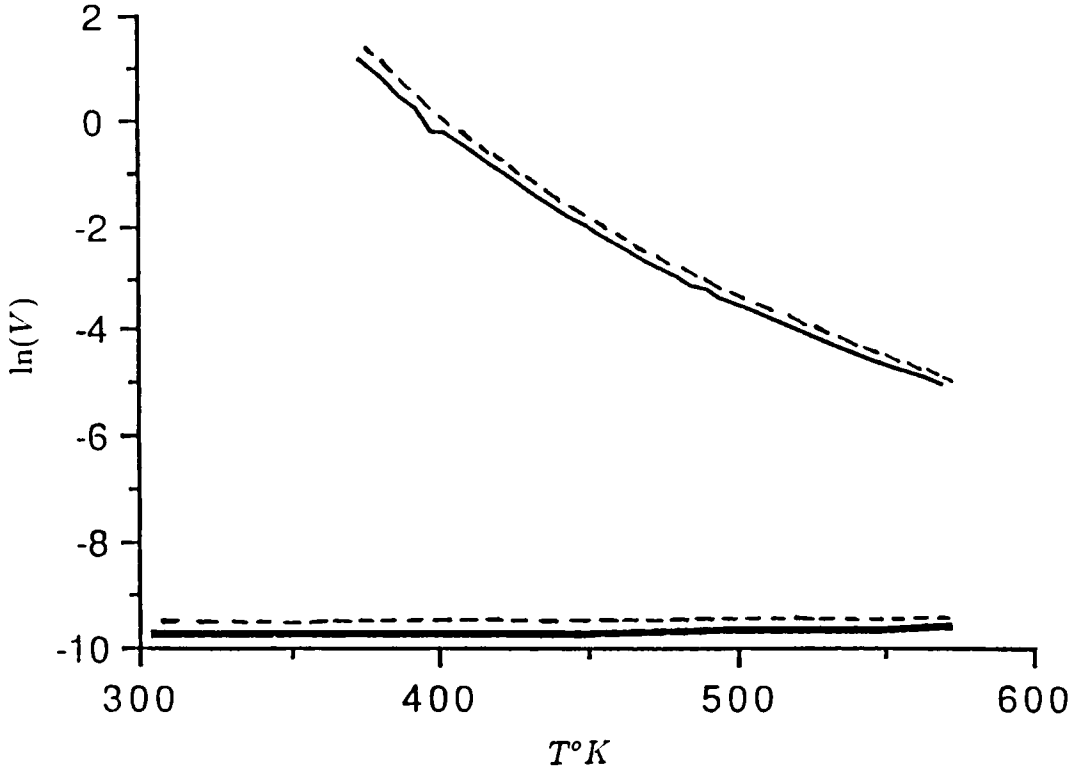


Figure 4.1: Orthobaric projection of the $T, \ln(V)$ surfaces of $(CH_2OH)_2/(CH_2OD)_2(- : (CH_2OH)_2, -- : (CH_2OD)_2)$

495 K [54] and above it $P^0(D_2O) > P^0(H_2O)$. The difference in the liquid molar volume between D_2O and H_2O decreases upto 378 K above which it increases sharply. At about 623 K the volume of heavy vapor is approximately 5 percent less than the volume of the light vapor.

If we now extend both the branches shown in Fig. 4.1 towards higher temperatures (approaching T_c') and incorporate the two cross over phenomenon, the temperature dependence of the MVIE leads us to predict the isotope effect on the critical temperature as positive *i.e.*, $T_c' > T_c$ as can be seen in Fig. 4.2. The prediction is in accord with previous observation [54].

Theoretical understanding of the lower branch in Fig 4.1 will be possible from a proper understanding of the isotope effect on the coefficient of thermal expansion, $\Delta\alpha$. Quantitative evaluation is possible by expressing the MVIE at some high temperature T_2 in terms of the known MVIE at a lower temperature T_1 by using appropriate integrals over compressibility and thermal expansivity

$$\ln(V^{0\prime}/V^0)_2 - \ln(V^{0\prime}/V^0)_1 = -\int_{P_1^0}^{P_2^0} \Delta\kappa_1 dP + \int_{T_1}^{T_2} \Delta\alpha dT - \int_{P_1^{0\prime}}^{P_1^0} \kappa_1' dP + \int_{P_2^{0\prime}}^{P_2^0} \kappa_1' dP. \quad (4.18)$$

In the numerical evaluation of the above Eqn. the term $\int_{T_1}^{T_2} \Delta\alpha dT$ dominates. From the previous discussion on the isotope effect on α we recall that only the isotope dependent high frequency vibrations and their anharmonicities contribute to $\Delta\alpha$. As temperature increases towards T_c' the properties of the liquid and the vapor become similar. The Gruneisen coefficient γ_i is small and it's

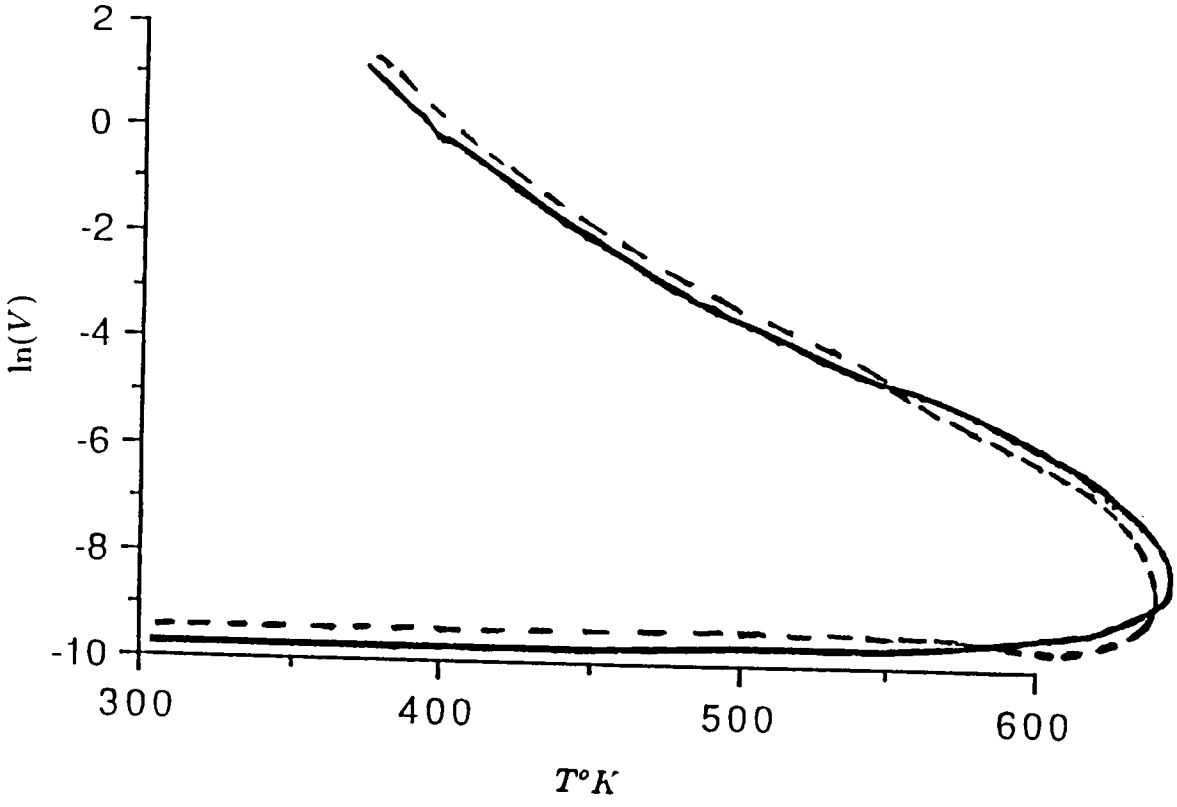


Figure 4.2: Extension of the orthobaric projection of the T, $\ln(V)$ towards T_c

temperature coefficient ($d\gamma_i/dT$) is small and negative. The negative sign of the pressure coefficient and its temperature coefficient establishes that the MVIE will cross over and become inverse once κ becomes large enough. Comprssibility becomes large as T_c' is approached and the product $\kappa(d\gamma_i/dT)$ (Eqn. 4.13) is significant.

The present observations on ethylene glycol are consistent with literature data on C_6H_6/C_6D_6, $(CH_3)_2CO/(CD_3)_2CO$, CH_3OH/CH_3OD [36], CH_4/CD_4 [71] and H_2O/D_2O [72,73]. These are the only other liquids where the MVIE and VPIE measurements have been made over a wide temperature range extending to the critical region. $\ln P^{0'}/P^0$ for ethylene glycol, like water and methanol, shows a complicated temperature dependence.

RPFR like VPIE starts large and positive at low temperatures and decays rapidly towards high temperature. The interpretations of their temperature dependences are straight forward. They are connected with the loss of hydrogen bonding as temperature increases.

The molecular basis of the MVIE has been discussed [43,35,41]. Contributions from both the intra– and intermolecular frequencies must be considered. The intermolecular contribution is often described in terms of a molecular size or steric effect. It's origin lies in the fact that rms averaged bond lengths for XH and XD are not the same due to the isotope effects on the mean–square amplitudes of molecular vibrations. The external contribution is related to the motions of the molecule itself and may include important anharmonic terms in

the potential. These, along with the amplitude effects, may lead to interesting temperature dependences for MVIE's [35]. Within the framework of the Born–Oppenheimer approximation the inter and intra–molecular potentials are isotope independent, so the MVIE can be described in terms of the isotope effects on the oxygen amplitudes. In other words, the unit cell volume can be uniquely defined in terms of the $O-O$ distance alone. Therefore the H/D effect on that volume may be determined by calculating the H/D effect on the $O-O$ distance through the amplitude effects.

The inverse MVIE on substitution at OH has been interpreted by Dutta–Choudhary and Van Hook [74]. It is associated with the librational motion of the particles in the hydrogen bonded network. The center of mass and center of interaction (about which the molecule vibrates) do not coincide and coupling effects must be taken into account. At higher temperatures the MVIE falls of to more negative values due to the combined effect of the ever increasing isothermal compressibilities which become unbounded at T_c, and the anharmonicity in the intramolecular degrees of freedom, especially the stretching modes.

In the above discussion we have compared the high temperature and pressure isotope effects on the PVT properties of ethylene glycol with those for liquids where the necessary measurements have been made. The MVIE temperature dependence and the predicted cross over behaviour close to T_c, establishes the IE on the critical temperature quite nicely. The κ isotope effect arises mainly from hard sphere contributions, whereas the thermal expansion IE is associated

primarily with high frequency isotope sensitive vibrations. The large isotope effects observed on the PV properties at high temperature are calculated from the VPIE and the low–temperature MVIEs.

4.2 Coexistence curve parameters and their isotope effects

In this section the pressure dependence and isotope effects on the coexistence curve parameters β, A, T_c, X_c, and dT_c/dP are discussed.

4.2.1 Critical Exponent β

β determines the limiting slope of the phase equilibrium line near the critical point and is theoretically expected to be a universal constant. Tests on a variety of systems have indicated the limiting value of β to be close to 0.33, which is also the value predicted by non–classical scaling theories. However, for experiments in the region of the phase diagram away from T_c, uncomplicated by long range fluctuations, mean field theory can be applied. Any mean field expression for phase coexistence when expanded around T_c gives a limiting exponent $\beta = 0.5$ as $T \rightarrow T_c$. This can be explained as follows. Any excess free energy function derived from theory is analytic in nature. As a result the derivatives of the free energy function are real and generally non zero at all points. This function can be expanded in a Taylor series around the critical point, T_c, which gives the result that as $T \rightarrow T_c$, $\beta = 1/2$. The two term $(\delta x, \delta T)$ expansion of free energy,

g, around g^c can be written as [75].

$$g = g^c + g_x^c(\delta x) = s^c(\delta T) - s_x^c(\delta x)(\delta T) - \frac{1}{2}s_{2x}^c(\delta x)^2(\delta T) + \frac{1}{24}g_{4x}^c(\delta x)^4 \quad (4.19)$$

From Eqn. 1.4 and Eqn. 1.5 the terms g_{2x}^c, g_{3x}^c and higher powers of (δT) are equal to zero. When we apply the Gibbs equilibrium conditions between the phases, *i.e.,* that the chemical potentials of each component between the two phases are equal, we get

$$(\delta x)' = -(\delta x)''$$

and

$$\frac{1}{6}g_{4x}^c(\delta x')^2 = \frac{1}{6}g_{4x}^c(\delta x'')^2 = s_{2x}^c(\delta T)$$

where $(\delta x) = (x_2 - x_2^c)$ and $'$ and $''$ represents the two phases. Thus

$$(\delta x) = (6s_{2x}^c/g_{4x}^c)^{1/2}(\delta T)^{1/2}$$

or

$$\beta = 1/2$$

The classical approach is appealing because it can predict T_c and critical amplitude. Non–ideality and consequent phase separation are due to non–zero excess free energies. The simplest representation for excess free energy is the one term Redlich–Kister expansion defining a regular mixture [61,76]

$$G^e = (X - X^2)B, \quad (4.20)$$

which gives a coexistence curve that is parabolic and centered at $X_c = 0.5$ and $T_c = B/(2R)$. A three or more term Redlich–Kister expansion

$$G^e = (X - X^2)\left[B_1 + B_2(1-2X) + B_3(1-2X)^2 + \cdots\right] \qquad (4.21)$$

can be used to account for the real shape of the coexistence curve, not centered at $X_c = 0.5$.

Application of the coexistence condition

$$(dG/dX)_{x'} = (dG/dX)_{x''}$$

to Eqn. 4.20 and Eqn. 4.21 gives an equation for the coexistence curve

$$\begin{aligned} RT \ln\left\{\frac{x'(1-x'')}{x''(1-x')}\right\} &= 2B_1(x' - x'') + \\ & 6B_2\left[(x' - x'') - (x'^2 - x''^2)\right] + 2B_3 \\ & \left[5(x' - x'') - 12(x'^2 - x''^2) + 8(x'^3 - x''^3)\right] \end{aligned} \qquad (4.22)$$

The applications and implications of such a treatment are explained in detail elsewhere [23].

We have used our coexistence data and least square analysis to extract the B_i parameters. In this fit we have used $x' = 2X_c + a(T_c - T) - x''$, to account for the non–symmetrical shape of the curve around X_c. a was extracted from the fit. Therefore Equation 4.22 amounts to a four parameter representation of our experiment, since we have fixed the observed maximum as X_c and T_c to reduce the dimensionality. The parameters of our fit are reported in Table 4.3. The parameters of the alternative scaling fit (Eqn. 3.34) were reported in Table 3.11

Table 4.3: Fits of phase separation data for $(CH_2OH)_2 + CH_3NO_2$ with classical expression

# of data points	135 (multiple)
T_c (max)	0.1
T_c/K	313.099
X_c	0.365
B_1/J mol^{-1}	6378.04 ± 11.74
B_2/J mol^{-1}K^{-1}	84.31 ± 24.46
B_3/J mol^{-1}K^{-1}	1477.61 ± 18.07
a	$0.01906 \pm 1.168 \times 10^{-3}$
$\sigma^2(T)$	0.0036
δx (classical)	0.03
δx (scaling)	0.05

on page 65. To decide which of the fits is the better representation we have computed the variance in T from the classical fit and then translated it into the error in the concentration by using the non–classical (scaling) form of the fit. We find that the error in concentration thus obtained is quite comparable to that computed directly from the scaling fit. That is to say, that over the entire temperature range both the representations work comparably. We do not have enough data points in the region $t < 10^{-3}$ at 1 atmosphere to be able to test the two formalisms with points very close to T_c(within the limiting region) at a single pressure.

These observations and earlier discussions [23] indicate that it is useful to distinguish between the empirically observed liquid–liquid coexistence points and the nonclassical and classical representations. Close to (T_c, X_c), nonclassical theory predicts the observed curvature in (T, X) but for $t_g > 10^{-3}$ (the Ginzberg limit [21]) the classical representation is adequate. The Ginzberg limit is a length scale that seperates classical and non–classical criticality. It determines how close to the transition, true critical behaviour is revealed. The classical theory also sufficiently represents the pressure dependence of (T_c, X_c).

It would be appropriate to include an interesting observation at this point. While the scaling Eqn. 1.6 yields β(apparent) = 0.33 for several binary systems, for some others it does not. Table 4.4 lists various systems found in the literature which yield β (apparent) 0.5. These data, like ours, extend over a broad temperature range. It is useful to be able to apply equilibrium thermodynamics

Table 4.4: UCST Parameters For Some Solutions

Solution (X_1/X_2)	T_c	$X_{1,c}$	β
$CH_3NO_2/(CH_2OH)_2$	313.10	0.64	0.51[a]
C_6H_{12}/CH_3OH	318.81	0.49	0.33[b]
C_6H_{12}/CH_3CN	349.79	0.47	0.33[c]
C_7F_{16}/CCl_4	330.88	0.42	0.32[d]
C_8H_{18}/CH_3NO_2	381.9	0.33	0.43[e]
$C_{11}H_{24}/CH_3NO_2$	403.55	0.23	0.51[f]
$C_{12}H_{26}/CH_3NO_2$	408.8	0.24	0.54[g]
C_4H_9NO/C_7H_{16}	358.6	0.499	0.35[h]
C_7F_{14}/C_7H_{16}	299.42	0.50	0.45[i]
$C_2H_4O_2/C_5H_{10}$	254.0	0.505	0.24[j]

[a] This work

[b] Van Hook A, Singh R: J. Chem. Phys., 87(10), 6097 (1987).

[c] Vani, Gopal, Guha: J. Chem. Phys., 86, 3999 (1986).

[d] Jacobs: J. Chem. Phys., 86, 1985 (1982).

[e] Malesinska: Int. Data Series. (1960)

[f] Maronglu, B: Int. Data Series. (1985)

[g] Young, C. L.: Int. Data Series. (1976)

[h] Spinolo, G: Int. Data Series. (1975)

to experimental systems over as wide a range as possible. Most theories which correlate thermodynamic properties with molecular structure and molecular parameters are mean field theories. Thus it is important to accurately determine the extent of the regions where the non–classical scaling and mean field theories apply. Only then is one assured that our non–classical or thermodynamic theories or models are being properly tested. Singh and Van Hook [23] have discussed the range of applicability for scaling, concluding in agreement with other authors that for $t > t_g$ ($t_g \approx 10^{-3}$ or less), the application of classical mean field theory is appropriate. The Redlich–Kister expansion of the free energy is widely used to describe non electrolyte mixtures. Moreover, recent work from Pitzer's laboratory [13,14,15] indicates that certain electrolyte solutions which phase separate are well described with $\beta = 0.5$, even close to (X_c, T_c). It is also suggested that the differences in coexistence curve pattern are related to the range of interparticle forces in both the near–critical and wide–ranging region [77]. This trend of apparent β with range of interparticle potential is very interesting and should be included in one's thinking about phase separation in fluids.

To summarize, β for ethylene glycol + nitromethane is independent of pressure and isotopic substitution. This result is in conformity with those observed for isobutyric acid + water [8] and cyclohexane + methanol [9,28].

4.2.2 Critical Concentration X_c

The value of X_c obtained is 0.365 (mole fraction ethylene glycol). There is no significant dependence on pressure for X_c, *i.e.*, $dX_c/dP \simeq 0$. We find no isotope effect on X_c. Both these results are consistent with those reported for other binary systems.

4.2.3 Critical Temperature T_c

The variation of T_c with isotopic substitution was first reported by Rabinovitch [26]. The observed IE on T_c for $(CH_2OH)_2((CH_2OD)_2) + CH_3NO_2$ system is $\Delta T_c = -2.05K$. The sign of the effect is in agreement with the qualitative analysis of Rabinovitch [26], but the magnitude is not [29]. He reports $\Delta T_c = -6.9K$. The only possible reason that we can suggest for this discrepency is the presence of moisture in the deuterated samples in the older study, since UCST increases by 2mK/ppm of water [19].

The condensed phase isotope effect (CPIE) theory pioneered by Bigeleisen [37] and extensively used by Van Hook and Jansco [31] offers a framework to explain CST IE's in terms of molecular structure and vibrational frequency shifts [56]. The approach, in useful approximation proceeds as follows. The molar excess free energy for a mixture of two components in the mole fraction ratio $x_1 : x_2$

$$A^e = -RT\left[x_1 \ln\left(\frac{Q_1}{Q_1^0}\right) + x_2 \ln\left(\frac{Q_2}{Q_2^0}\right)\right]. \tag{4.23}$$

Component 2 when replaced by the isotopic analog 2′ gives,

$$A^{e'} = -RT\left[x_1 \ln\left(\frac{Q_1}{Q_1^0}\right) + x_2 \ln\left(\frac{Q_2'}{Q_2^{0'}}\right)\right]. \tag{4.24}$$

Equations 4.23 and 4.24 are combined to give an expression for $\Delta T/T$ in terms of the partition function ratio (RPFR).

$$\Delta T/T = \ln\left[\frac{Q_2'/Q_2}{Q_2^{0'}/Q_2^0}\right] \tag{4.25}$$

Referring to section 1.3 in the introduction, for symmetrically substituted isotopic molecules, Eqn. 4.25 reduces to

$$\Delta T/T = \ln\left[\frac{f_c}{f_{soln}}\right]$$

The partition function ratio is then given by

$$\ln\left[\frac{Q_2'/Q_2}{Q_2^{0'}/Q_2^0}\right] = \ln\left\{\prod_{i=1}^{3n} \frac{\left[\frac{\exp(-u_i'/2)}{1-\exp(-u_i')}\right]^c \left[\frac{\exp(-u_i/2)}{1-\exp(-u_i)}\right]^s}{\left[\frac{\exp(-u_i'/2)}{1-\exp(-u_i')}\right]^s \left[\frac{\exp(-u_i/2)}{1-\exp(-u_i)}\right]^c}\right\}. \tag{4.26}$$

The superscripts c and s refer to pure condensed phase and dilute solution respectively. For the case where the vibrations fall into two classes, one of which can be treated in the low temperature (B term) and the other in the high temperature approximation (A term), Eqn. 4.26 reduces to

$$\frac{\Delta T}{T} \simeq \frac{1}{24}\left(\frac{hc}{kT}\right)^2 \left[\sum_{ext}(\nu_{soln}'^2 - \nu_{soln}^2) + \sum_{ext}(\nu_c'^2 - \nu_c^2)\right] + \frac{hc}{2kT}\left[\sum_{int}(\nu_{soln}' - \nu_{soln}) + \sum_{int}(\nu_c' - \nu_c)\right]. \tag{4.27}$$

where the subscript c's refer to the pure liquid standard states. Equation 4.27 is the familiar AB Eqn. 1.13.

This formalism implies that the isotope effect is a function of the frequency shift of the main bond stretching motions as well as of the non–negligible librational motions on transfer from pure liquid to solution. We can not evaluate the isotope effects exactly since the complete vibrational assignments of the frequency shifts of ethylene glycol or nitromethane into ethylene glycol + nitromethane solution are not available. However we can make some crude calculations from information available on OH bond stretching frequencies. An approximate model put forth for OH/OD substitution [9] applies the mean field theory of Guggenheim for symmetrical mixtures [30] wherein, an excess thermodynamic property of interest *e.g.* G^e is given by

$$G^e = (X - X^2)\left[B_g - B_g^2(X - X^2)/(zRT) + \cdots\right]$$

where z is the co–ordination number in the pseudo lattice employed to evaluate the statistical thermodynamic problem. Applying the critical condition one obtains

$$d^2G/dX^2 = 0 = 4RT_c - 2B_g - \frac{2B_g^2}{zRT}(1 - 6X + 6X^2).$$

On differentiating with respect to isotope we obtain

$$\frac{\Delta T_c}{T_c} = \frac{\Delta B_g}{B_g}\frac{zm_z - 4}{zm_z - 2}$$

where B_g is the partial molar free energy of transfer from the pure reference liquid to the infinitely dilute solution and $m_z = (1 \pm \sqrt{1 - 4/z}$. This model

further gives

$$\frac{T_c(\mathrm{H}) - T_c(\mathrm{D})}{T_c(\mathrm{H})} = \frac{W}{4}\left\{\frac{hc}{2kT}\delta\nu_{\mathrm{OH}}\left[1 - \left(\frac{\mu_{\mathrm{OH}}}{\mu_{\mathrm{OD}}}\right)^{1/2}\right] + 2\mathrm{LIB}((CH_2OD)_2)\right\} \quad (4.28)$$

where $W = W'm_z$, $W' = (zm_z - 4)/(zm_z - 2)$. The internal vibrations of the OH and the CH_2 groups and the skeletal vibrations of $(CH_2OH)_2$ and $(CH_2OD)_2$ have been recorded [62,65] in the liquid state and are listed in Table 4.1 on page 73. Measurements and analysis of infrared spectra of $(CH_2OH)_2$ and $(CH_2OD)_2$, isolated in Ar and Xe matrices indicate the existence of one free and one internally bonded OH group in both conformers [78]. This internal H bonding produces a relatively small shift $\Delta\nu = \nu(\mathrm{OH})_{free} - \nu(OH)_{tonded} \approx 35cm^{-1}$. This separation is also confirmed from studies of the ethylene glycol spectra in dilute CCl_4 solution [64].

The two librational vibrations (1405 and $700cm^{-1}$) should be considered. The librational contribution is calculated from Eqn. 4.26 because for these librational frequencies which shift from 1405 to $974cm^{-1}$ and 700 to $450cm^{-1}$ on transfer from the hydrogen bonded liquid to non polar solvent, the AB approximation is inadequate. The external translations can be ignored because they are small and not much affected by isotopic substitution. The OH stretches blue shift [79] by approximately $-300cm^{-1}$ in non polar solvents. This is consistent with the observed frequencies [62,78,64]; $\nu(\mathrm{OH})_s = 3644cm^{-1}$, $\nu(\mathrm{OH})_c = 3275cm^{-1}$, $\nu(\mathrm{OD})_s = 2682cm^{-1}$, and $\nu(\mathrm{OD})_c = 2475cm^{-1}$. $z = 4.012$

is calculated from Eqn. 4.29

$$z = \frac{(B_1 + B_3)^2}{4RTB_2}, \tag{4.29}$$

where the B_i parameters are listed in Table 4.3 on page 92. With these approximations we obtain $\Delta T/T = -0.0075$. The experimental $\Delta T/T = -0.006$. The agreement is acceptable in view of the approximations employed.

4.2.4 Critical Amplitude A

The width of the coexistence curve is determined by the critical amplitude A. Referring to Table 3.11 on page 65 we see no pressure dependence over the present pressure range. The value of A empirically defined by fitting data to the scaling relation is highly sensitive to the range and distribution of data points over $0 < t < t(max)$. Interlaboratory comparisons are therefore difficult because different workers very rarely choose similar ranges. The experimental A's show a standard deviation of $\sim 10\%$. This is consistent with the results reported by Scott [60], Singh [9], Woerman [28], and Greer [8]. The scaling law literature gives no explaination on what determines A except that the various critical amplitudes are related to each other with certain universal constants(two–scale–factor–universality hypothesis).

Classical thermodynamics can be used to understand the IE on the amplitude. The symmetric mixture of Guggenheim [30] is described by

$$g^e = x(1-x)(\alpha + B(1-2x)^2) \tag{4.30}$$

where the higher order term is added to improve the fitting of the data. B serves to flatten the top of the coexistence curve similar to the fashion in which β governs the flatness of the curve in the scaling equation. It has been shown [9] that if the ratio α/B is fixed, Eqn. 4.30 can reproduce the coexistence curve.

Applying 2–phase equilibrium conditions for a symmetric mixture

$$\left(\frac{\partial g^1}{\partial x}\right)_{x_e^1} = \left(\frac{\partial g^2}{\partial x}\right)_{x_e^2} = \frac{\Delta_e g}{\Delta_e x} \tag{4.31}$$

then reduces to

$$RT \ln \frac{x'}{1-x'} = -\left(\frac{\partial g^e}{\partial x}\right)_{x_e'}$$

From Eqn. 4.30

$$-\left(\frac{\partial g^e}{\partial x}\right)_{x_e'} = 2\alpha x + 2B(x(1-2x)^2 + 2(1-2x)^2)$$

Substituting $x = x_c - At^\beta$ we get

$$RT \ln \frac{X_c - At^\beta}{X_c + At^\beta} = 2\alpha\left(X_c - At^\beta\right) + 2B\left(\left(X_c - At^\beta\right)\left(2At^\beta\right)^2 + 2\left(At^\beta\right)^2\right). \tag{4.32}$$

It is seen therefore that A is a function of the free energy parameters α ($\alpha = 2RT_c$) and B. Thus if there is an isotope effect on the critical solution temperature there would also be an isotope effect on A. The literature shows little or no information on the nature of A and its isotope effect.

4.2.5 Slope of the Critical Line dT_c/dP

The slope of the critical line $c = (dT_c/dP)$ is $0.0016 \pm 4.0 \times 10^{-5} K/bar$. There is no prior literature on the pressure dependence for the coexistence curve of

this system, hence a comparison is not possible. The slope is independent of pressure and isotopic substitution within the experimental precision. dT_c/dP can be estimated from theory in the following manner.

An equation first obtained by Scott [80] for strictly regular solutions can be used to obtain a value for the critical slope if v^e and h^e are known for the mixture at the critical point.

$$dT_c/dP = \frac{Tv^e}{h^e} \tag{4.33}$$

Equation 4.33 has been used by Clerke [81] (3–methyl pentane + nitroethane), Benson [82] (methyl cyclohexane + tetradecafluoromethyl cyclohexane) and Singh [56] (cyclohexane + methanol) quite successfully. Search of standard references [57,83] shows that very little thermodynamic data is available on this system. Hence we cannot apply these theoretical methods to our system.

Another method derived by Griffiths and Wheeler [84] yields

$$dT_c = T\left(\frac{1/V dV/dT}{\rho_c C_{p,x}}\right) \tag{4.34}$$

where ρ_c is the critical density, and $C_{p,x}$ is the specific heat per unit mass. Applying scaling laws and the two–scale universality hypothesis [85,86] their approach gives

$$\frac{dT_c}{dP} = \frac{T\nu\alpha}{k_B}(\zeta_0/0.27)^3.$$

ζ_0 being the critical amplitude for the correlation length [22] and 0.27 being the universal amplitude ratio for fluids as obtained from RG techniques [22]. α is another critical exponent whose value is generally accepted as 0.11. ν

is the correlation length exponent and k_B is the Boltzmann's constant. It is observed [56] that regular solution theory underestimates the magnitude of the slope while scaling laws overestimate the effect; though the sign and order of magnitude are correct in both cases.

There is no measurable isotope effect on dT_c/dP. It can be obtained from Eqn. 4.33 as

$$\frac{\Delta dT_c/dP}{dT_c/dP} = \frac{\Delta T_c}{T_c} + \frac{\Delta v^e}{v^e} - \frac{\Delta h^e}{h^e} \cdots$$

if the isotope effects on v^e and h^e are available. A 20% isotope effect has been found for the slope for the isobuteric acid + water system [28] but none for cyclohexane + methanol [56]

There is a first order linear dependence on pressure for the critical solution temperature upto $50MPa$. Greer [8], Clerke [81], Benson [82], and Singh [56] all report a linear dependence of T_c on pressure. All these data extend only upto $13MPa$. A curvature has been observed for systems studied at $300MPa$ [87]. A fit of our data to Eqn. 1.8 in which $T_c = T_c, 0 + aP + bP^2$ we obtain $b = 1.183 \times 10^{-6} \pm 2.9 \times 10^{-7} Kbar^{-2}$. The possibility of curvature at higher pressures cannot be ruled out. A happy coincidence is that Lichtenthaler [87] reports $b = 2 \times 10^{-6} Kbar^{-2}$ for the 2–methoxyethanol + hexane system.

CHAPTER 5

Conclusion

The thrust of this thesis is mainly experimental. We have studied the co–existence curve of the ethylene glycol and nitromethane system and investigated the effect of pressure and isotopic substitution on the same. As is obvious from the sparsity of literature data in this system it is being studied with some detail for the first time for both the systems $((CH_2OH)_2 + CH_3NO_2)$ and $((CH_2OD)_2 + CH_3NO_2)$ The results have been rationalized on the basis of simple models and by using scaling laws as well as classical thermodynamics.

For both the systems the critical exponent β is 0.507 ± 0.028. The coexistence curve for the whole temperature range $0 < t < 0.1$ is described equally well by the scaling laws as well as mean field theory expressions. β is independent of pressure. The critical concentration X_c was also found to be independent of pressure and isotopic substitution. The slope of the critical line dT_c/dP is also invariant under pressure and isotopic substitution. The isotope effect on the critical solution temperature $\Delta T_c = T_{c,H} - T_{c,D}$ is negative. There is an isotope effect on the critical amplitude. These results are in conformity with those obtained for other binary systems for which such precise measurements have been done. We have also briefly outlined some methods to rationalize

experimental data of this kind by using the theory of condensed phase isotope effects.

Vapor pressures, liquid compressibilities, expansivities, and molar volumes have been measured at high precision for $(CH_2OH)_2$ and $(CH_2OD)_2$ from room temperature upto 574^oK. These various results are compared with data for other systems and are discussed in terms of the statistical theory of isotope effects in condensed phases. We have tried to confirm that high temperature MVIE behaviour does indeed lead to prediction of the correct isotope effect on the critical temperature. This could be established if the same measurements are continued upto the critical temperature. Vapor nonideality corrections led to a correct prediction of the VCIE. High temperature PV properties of fluids show large isotope effects which can be calculated from the VPIE and the low temperature MVIE's. A complete application of the well established theory of condensed phase isotope effects will be possible when extensive spectroscopic information on ethylene glycol becomes available.

There is a great interest in isotope effects in phase separation phenomenon and condensed phase properties as witnessed by the large number of publications found in the literature. It is hoped that this work will contribute towards formulating a correlation between the two effects.

BIBLIOGRAPHY

BIBLIOGRAPHY

[1] G. E. Uhlenbeck, "Critical Phenomenon," in *National Bureau of Standards Miscellaneous Publication*, (M. S. Green and J. V. Sengers, eds.), p. 273, Washington: National Bureau of Standards, 1966.

[2] K. G. Wilson, "Renormalisation Group and Critical Phenomena: The Kadanoff Scaling Picture," *Phys. Rev. B*, vol. 4, p. 3174, 1971.

[3] K. G. Wilson, "Renormalisation Group and Critical Phenomena: Phase–Space Cell Analysis of Critical Behavior," *Phys. Rev. B*, vol. 4, p. 3184, 1971.

[4] K. G. Wilson and M. E. Fisher, "Critical Exponents in 3.99 Dimensions," *Phys. Rev. Letters*, vol. 28, p. 240, 1972.

[5] C. Domb, "Critical Phenomena: A brief Historical Survey," *Contemp. Phys.*, vol. 26, p. 49, 1985.

[6] J. de Heer, *Phenomenological Thermodynamics.* Englewood Cliffs,N.J.: Prentice–Hall, 1986.

[7] S. C. Greer, "Coexistence Curves at Liquid–Liquid Critical Points: Ising Exponents and Extended Scaling," *Phys. Rev. A*, vol. 14, p. 1770, 1976.

[8] S. C. Greer, "Coexistence Curve of D_2O+ Deuterated Isobutyric Acid," *Ber. Bunsenges. Phys. Chem.*, vol. 8, p. 1079, 1977.

[9] R. R. Singh and W. A. Vanhook, "The effect of H/D substitution and Pressure on the Liquid–Liquid Equilibrium Between Cyclohexane and Methanol," *J. Chem. Phys.*, vol. 87, no. 10, p. 6097, 1987.

[10] V. Vani, E. S. R. Gopal, and S. Guha, "Coexistence Curve of Acetonotrile and Cyclohexane Liquid System," *J. Chem. Phys.*, vol. 84, p. 3999, 1986.

[11] E. S. R. Gopal, R. Ramachandra, P. Chandrasekhar, K. Govindarajan, and S. V. Subramanyam, "Critical Exponent β and Rectilinear Diameter of the Binary– Liquid System Carbon Disulfide + Nitromethane," *Phys. Rev. Lett.*, vol. 32, p. 284, 1974.

[12] D. T. Jacobs, "Coexistence Curve of a Nonpolar Binary Fluid Mixture. Perfluoroheptane–Carbon Tetrachloride," *J. Phys. Chem.*, vol. 86, p. 1895, 1982.

[13] K. S. Pitzer, " Some Interesting Properties of Vapor–Liquid or Liquid–Liquid Coexistence Curves for Ionic and Non–Ionic Fluids," *Thermochimica Acta*, vol. 139, p. 25, 1989.

[14] K. S. Pitzer, "Large–Scale Fluctuations and the Critical Behaviour of Dilute NaCl in H_2O," *J. Phys. Chem.*, vol. 90, p. 1502, 1986.

[15] K. S. Pitzer, M. C. P. de Lima, and D. R. Schreiber, "Critical Point and Phase Separation for an Ionic System," *J. Phys. chem.*, vol. 89, p. 1854, 1985.

[16] J. Timmermans, *Les Solutions Concentrees.* Paris: Masson et Cie, 1936.

[17] J. L. Tveekrem and D. T. Jacobs, "Impurity Effects in a Near–Critical Binary–Fluid Mixture," *Phys. Rev. A*, vol. 27, p. 2773, 1983.

[18] R. H. Cohn and D. T. Jacobs, "Acetone Impurity Effects on the Binary Fluid Mixture Methanol– Cyclohexane," *J. Chem. Phys.*, vol. 80, p. 856, 1984.

[19] R. R. Singh and W. A. V. Hook, "Effect of Dissolved Gas on the Critical Solution Temperature of (Cyclohexane + Methanol)," *J. Chem. Therm.*, vol. 18, p. 1021, 1986.

[20] A. Stein and G. F. Allen, "An Analysis of Coexistence Curve Data for Several Binary Liquid Mixtures Near Their Critical Points," *J. Phys. Chem. Ref. Data*, vol. 2, p. 443, 1973.

[21] V. L. Ginzberg, "Some Remarks on Phase Transitions of the Second Kind and the Microscopic Theory of Ferroelectric Materials," *Fizika Tela*, vol. 2, p. 2031, 1960.

[22] A. Kumar, H. R. Krishnamurthy, and E. S. R. Gopal, "Equilibrium Critical Phenomena In Binary Liquid Mixtures," *Phys. Reports*, vol. 98, p. 57, 1983.

[23] R. R. Singh and W. A. V. Hook, "Comments on Classical and Nonclassical Representations of Critical Demixing in Liquid–Liquid Binary Solutions," *J. Chem. Phys.*, vol. 87, p. 6088, 1987.

[24] M. Gordon and J. A. Torkington, "Scrutiny of the Critical Exponent Paradigm, As Exemplified By Gelation," *Pure and Appl. Chem.*, vol. 53, p. 1461, 1981.

[25] N. F. Hall, H. R. Wentzel, and T. Smith, "Liquid–Liquid Equilibria Involving Heavy Water," *J. Am. Chem. Soc.*, vol. 56, p. 1822, 1934.

[26] I. B. Rabinovitch and V. G. Tsvetkov, "The Opposed Effects of the Substitution of Hydrogen by Deuterium on the Dissociation Energy of the Hydrogen Bond and the Van der Waals Interaction Energy," *Russ. J. of Phys. Chem.*, vol. 45, p. 458, 1970.

[27] D. V. Fenby, Z. S. Kooner, and J. R. Khurma, "Deuterium Isotope Effects In Liquid–Liquid Phase Diagrams: A Review," *Fluid Phase Equilibria*, vol. 7, p. 327, 1981.

[28] W. Schon, R. Wiechers, and D. Woermann, "Deuterium Isotope Effects in Binary Critical Mixtures," *J. Chem. Phys.*, vol. 85, p. 2922, 1986.

[29] V. G. Tsvetkov and I. B. Rabinovitch, "Isotope Effect in the Consolute Temperatures for a Number of Substances in Deuterium Oxide and Deuterio Ethylene Glycol," *Russion J. of Phys. Chem.*, vol. 47, No. 9, p. 1355, 1973.

[30] E. A. Guggenheim, *Applications of Statistical Mechanics*. Clarendon, Oxford: Prentice–Hall, 1966.

[31] G. Jansco and W. A. V. Hook, "Condensed Phase Isotope Effects (Especially Vapor Pressure Isotope Effects)," *Chem. Rev.*, vol. 74, p. 689, 1974.

[32] W. A. V. Hook, "Isotope Effects in Condensed Phases, the Benzene Example. Influence of Anharmonicity; Harmonic and Anharmonic Potential Surfaces and Their Isotope Independence. Molar Volume Isotope Effects in Isotopic Benzenes," *J. Chem. Phys.*, vol. 83, p. 4107, 1985.

[33] S. Matsuo and W. A. V. Hook, "Isothermal Compressibility of $C_6H_{12}, C_6D_6, c-C_6H_{12}, c-C_6D_{12}$, and Their Mixtures from 0.1 to 35 MPa at 288, 298, and 313 K," *J. Phys. Chem.*, vol. 88, p. 1032, 1984.

[34] Z. S. Kooner and W. A. V. Hook, "Apparatus To Measure Vapor Pressure, Differential Vapor Pressure, Liquid Molar Volume and Compressibility of Liquids and Solutions to the Critical Point. Vapor Pressures, Molar Volumes, and Compressibilities of Protiobenzene and Deuteriobenzene at Elevated Temperatures," *J. Phys. Chem.*, vol. 90, p. 4860, 1986.

[35] F. Menes, T. Dorfmuller, and J. Bigleisen, "Molar Volumes of the Isotopic Homologs of Ethylene," *J. Chem. Phys.*, vol. 53, p. 2869, 1970.

[36] Z. S. Kooner and W. A. V. Hook, "Isotope Effects of Simple Fluids," *J. Phys. Chem.*, vol. 92, p. 6414, 1988.

[37] J. Bigeleisen, "Statistical Mechanics of Isotope Effects on the Thermodynamics Properties of Condensed Systems," *J. Chem. Phys.*, vol. 34, p. 1485, 1961.

[38] J. Bigeleisen and M. G. Mayer, "Calculation of Equilibrium Constants for Isotope Exchange Reactions ," *J. Chem. Phys.*, vol. 15, p. 261, 1947.

[39] M. J. Stern, W. A. V. Hook, and M. Wolfsberg, " Isotope Effects on Internal Frequencies in the Condensed Phase Resulting from Interactions with the Hindered Translations and Rotation. The Vapor Pressures of the Isotopic Ethylenes ," *J. Chem. Phys.*, vol. 39, p. 3179, 1963.

[40] E. B. Wilson, J. C. Decius, and P. C. Cross, *Molecular Vibrations*. New York: McGraw–Hill, 1955.

[41] J. Bigleisen, S. V. Ribnikar, and A. V. Hook, "Molecular Geometry and the Vapor Pressure of Isotopic Molecules. The Equivalent Isomers *cis–*, *gem,* and *trans*–Dideuteroethylenes," *J. Chem. Phys.*, vol. 38, p. 489, 1963.

[42] J. Bigleisen, M. J. Stern, and A. V. Hook, "Molecular Geometry and the Vapor Pressure of Isotopic Molecules.C_2H_3D and $C^{12}H_2 = C^{13}H_2$," *J. Chem. Phys.*, vol. 38, p. 497, 1963.

[43] L. S. Bartell and R. R. Roskos, "Isotope Effects on Molar Volume and Surface Tension:Simple Theoretical Model and Experimental Data for Hydrocarbons," *J. Chem. Phys.*, vol. 44, p. 457, 1966.

[44] A. F. Grigor and W. A. Steele, "Physical Properties of Fluid CH_4 and CD_4: Experimental," *J. Chem. Phys.*, vol. 48, p. 1032, 1968.

[45] A. F. Grigor and W. A. Steele, "Physical Properties of Fluid CH_4 and CD_4: Theory," *J. Chem. Phys.*, vol. 48, p. 1038, 1968.

[46] J. Bigeleisen, S. V. Ribnikar, and W. A. V. Hook, "Molecular Geometry and the Vapor Pressure of Isotope Molecules. The Equivalent Isomers *cis–*, *gem–*, and *trans*–Dideuteroethylenes," *J. Chem. Phys.*, vol. 38, p. 489, 1963.

[47] D. Ambrose and D. J. Hall, "Thermodynamic Properties of Organic Oxygen Compounds," *J. Chem. Thermodynamics*, vol. 13, p. 61, 1981.

[48] O. J. Schierholtz and M. L. Staples, "Vapor Pressures of Certain Glycols," *Ontario Research Foundation*, vol. 57, p. 2709, 1935.

[49] C. A. Taylor and W. H. Rinkenbach, " Ethlene Glycol – An Evaluation of available Information on the Physical Properties of this Compound," *Ind. and Engg. Chem.*, vol. 18, p. 676, 1926.

[50] D. R. Stull, " Vapor Pressure of Pure Substances," *Ind. and Engg. Chem.*, vol. 39, p. 517, 1947.

[51] W. S. Jones and W. S. Tamplin, "Glycols," in *A.C.S Monograph Series*, (G. U. Curme and F. Johnson, eds.), Reinhold, New York: American Chemical Society, 1952.

[52] A. F. Gallaugher and H. Hibbert, "Studies on Reaction Relating to carhydrates and Polysaccharides LV. Vapor Pressures of Polyethylene Glycols and their Derivatives," *J. Am. Chem. Soc.*, vol. 59, p. 2521, 1937.

[53] " TRC Tables – Nonhydrocarbons," 1966.

[54] I. B. Rabinovitch, *Effect of Isotopy on the Physicochemical Properties of Liquids*. New York: Consultants Bureau, 1970.

[55] M. E. Fisher and P. E. Scesney, "Visibility of Critical–Exponent Renormalisation," *Phys. Rev. A*, vol. 2, p. 825, 1970.

[56] R. R. Singh, *Effect of H/D Substitution and Pressure on the Phase Equilibrium of Cyclohexane + Methanol* . PhD thesis, The University Of Tennessee, Knoxville, March 1987.

[57] " International Critical Tables of Numerical Data, Physics Chemistry and Technology," 1928.

[58] R. E. Gibson and O. H. Loeffler, " $P-V-T$ Relations in Solutions. V. The Energy Volume Coefficients of Carbon Tetrachloride, Water, and Ethylene Glycol ," *J. Amer. Chem. Soc.*, vol. 63, p. 898, 1941.

[59] P. N. Nikolaev and I. B. Rabinovitch, " Heat Capacity of Ethylene Glycol and Ethylene Deuterioglycol in the Temperature Range $80-300K$," *Russ. J. Phys. Chem.*, vol. 41, p. 1179, 1967.

[60] R. L. Scott, "Critical Exponent for Binary Fluid Mixtures," in *Chemical Thermodynamics - Specialist Periodical Reports*, (M. L. McGlashan, ed.), p. 238, London: The Chemical Society, 1978.

[61] J. Hildebrand, J. H. VanNostrand, and R. L. Scott, *The Solubilities of Non-electrolytes*. New York: Rheinhold, 1950.

[62] W. Sawodny, K. Niedenzu, and J. W. Dawson, " The Vibrational Spectrum of Ethylene Glycol ," *Spectrochim. Acta*, vol. 23A, p. 799, 1967.

[63] W. A. V. Hook and G. Jansco, " Vapor Pressure Isotope Effects in Benzene–Cyclohexane Systems. III. Theoretical Analysis ," *J. Chem. Phys.*, vol. 68, p. 3191, 1978.

[64] L. P. Kuhn, " The Hydrogen Bond. I Intra and Intermolecular Hydrogen Bonds in Alcohols ," *J. Amer. Chem. Soc.*, vol. 74, p. 2492, 1952.

[65] H. Matsuura and T. Miyazawa, " Infrared Spectra and Molecular Vibrations of Ethylene Glycol ," *Bull. Chem. Soc. Japan*, vol. 40, p. 85, 1967.

[66] J. F. H. Stillinger, "Compressibility of Simple Fused salts ," *J. Chem. Phys*, vol. 35(10), p. 1581, 1961.

[67] K. Arakawa and K. Kojima, "Investigation of the Concept of Free Volume by Means of a Correlation Function Method ," *Bull. Chem. Soc. Japan*, vol. 48(1), p. 26, 1975.

[68] G. E. Walrafen and M. Abebe, "Raman Studies of the Bending and Librational Bands from Water and Ice VI to $\approx 12kBar$ at $32°C$," *J. Chem. Phys.*, vol. 68, p. 4694, 1978.

[69] S. J. Cyvin, *Molecular Vibrations and Mean Square Amplitudes* . Amsterdam: Elsevier, 1968.

[70] J. O. Hirschfelder, C. F. Curtiss, and R. B. Bird, *Molecular Theory of Gasses and Liquids* . New York: John Wiley and Sons, Inc., 1954.

[71] A. Y. Fang and W. A. V. Hook, " Isotope Effects on the Vapor Phase Second Virial Coefficients of the Deuterated Methanes ," *J. Chem. Phys.*, vol. 60, p. 3513, 1974.

[72] G. S. Kell, G. E. McLaurin, and E. Whalley, " PVT Properties of Water. II. Virial Coefficients in the Range $150° - 450°C$ Without Independent Measurement of Vapor Volumes ," *J. Chem. Phys.*, vol. 48, p. 3805, 1968.

[73] G. S. Kell, G. E. McLaurin, and E. Whalley, " PVT Properties of Water. III. Virial Coefficients of D_2O in the range $150° - 500°C$," *J. Chem. Phys.*, vol. 49, p. 2839, 1968.

[74] M. K. Dutta–Choudhury and W. A. V. Hook, " Isotope Effects in Aqueous Systems. 11. Excess Volumes in H_2O/D_2O Mixtures. The Apparent Molar Volume of NaCl in an H_2O/D_2O Mixture ," *J. Phys. Chem.*, vol. 84, p. 2735, 1980.

[75] J. S. Rowlinson and F. L. Swinton, *Liquids and Liquid Mixtures*. London: Butterworth, 1982.

[76] E. A. Guggenheim, *Thermodynamics*. Amsterdam: North Holland, 1967.

[77] K. S. Pitzer, "Thermodynamic properties of Ionic fluids over wide ranges of temparature," *Pure & Appl. Chem.*, vol. 59, p. 1, 1987.

[78] H. Frei, T. H. A., R. Meyer, and H. H. Gunthard, "Ethylene Glycol: IR Spectra, AB Initio Calculations, Vibrational Analysis and Conformations Of 5 Matrix Isolated Isotopic Midifications ," *Chem. Phys.*, vol. 25, p. 271, 1977.

[79] V. Bekarek and A. Mikulecka, " A Note on Evaluation of Solvent Shifts in IR Spectroscopy ," *Coll. Czech. Chem. Comm.*, vol. 43, p. 2879, 1978.

[80] D. B. Myers, R. A. Smith, J. Katz, and R. L. Scott, "The Effect of Pressure on Liquid Miscibility," *J. Phys. Chem.*, vol. 70, p. 3341, 1966.

[81] E. A. Clerke, J. V. Sengers, R. A. Ferrell, and J. K. Bhattacharjee, "Pressure effects and ultrasonic attenuation in the binary liquid mixture 3–methylpentane and nitroethane near the critical point," *Phys. Rev. A*, vol. 27, p. 2140, 1983.

[82] M. K. Kumaran and G. C. Benson, "Effect Of Pressure On The Critical Solution Temperature Of (Methylcyclohexane + Tetradecafluoromethylcyclohexane)," *Fluid Phase Equilibria*, vol. 11, p. 13, 1983.

[83] " International Data Series: Selected Data on Mixtures A ," 1973–87.

[84] R. B. Griffiths and J. C. Wheeler, "Critical Points in Multicomponent Systems," *Phys. Rev. A*, vol. 2, p. 1047, 1970.

[85] E. A. Clerke, *Pressure Dependence on the Phase Diagram of the Binary System 3–MethylPentane + Nitroethane.* PhD thesis, University of Maryland, June 1982.

[86] R. B. Kopelman, R. W. Gammon, and M. R. Moldover, "Turbidity very near the critical point of methanol–cyclohexane mixtures," *Phys. Rev. A*, vol. 29, p. 2048, 1984.

[87] H. Bijl, T. W. D. Loos, and R. N. Lichtenthaler, " Liquid–Liquid Equilibrium in 2–Methoxyethanol + Alkane Systems: Experimental Results and Pressures upto 400MPa," *Fluid Phase Equil.*, vol. 22, p. 321, 1985.

APPENDIX

APPENDIX A

Calibration of Thermometers

Table A.1: Calibration of the platinum resistance thermometer (CST)

#	t_{68} in ^{o}C	R′ in Ohms
1	44.846	117.3768
2	44.844	117.3765
3	46.576	118.0429
4	46.575	118.0429
5	47.622	118.444
6	47.626	118.4445
7	48.381	118.7345
8	48.384	118.7346
9	48.952	118.9557
10	49.932	119.3405
11	49.934	119.3405
12	51.216	119.8379
13	52.243	120.2358
14	55.729	121.5789

Data fitted to equation $t_{68} = a + bR$
Least Squared parameters are
$a = -258.8877 \pm 0.02168$
$b = 2.58776 \pm 0.00182$
with a variance of function $= 7.8 \times 10^{-5}$

Table A.2: Calibration of the platinum resistance thermometer (PVT)

#	t_{68} in $^{\circ}C$	R′ in Ohms
1	29.993	111.79
2	51.7382	120.214
3	74.9074	129.119
4	99.6825	138.564
5	126.2515	148.623
6	150.7106	157.815
7	174.9397	166.852
8	199.8535	176.068
9	225.1517	185.368
10	249.8949	194.383
11	275.7773	203.78
12	300.2634	212.57

Data fitted to equation $t_{68} = a + bR + cR^2$
Least Squared parameters are

$a = 100.085351 \pm 0.007439$

$b = 259.264464 \pm 0.0688$

$c = 1.5794 \pm 0.008326$

with a variance of function $= 3.027 \times 10^{-4}$

Vita

Madhuri Vasant Salvi was born in Kolhapur, India, on July 11, 1960. She was raised in Pune, India where she completed her secondary education at St. Joseph's High School in 1977. She completed her B.Sc. in chemistry from Fergusson College, Pune University in 1980 and her M.Sc. in inorganic chemistry in 1982. She worked as a research chemist at the National Chemical Laboratory, Pune until June 1984.

In Fall 1984 she was admitted to the graduate program in chemistry at the University of Tennessee, Knoxville. She graduated with a Doctor of Philosophy in December 1989.

Madhuri and her husband Ravindra plan to stay in Knoxville while she does a stint of post doctoral research.